宿主細胞由来のRNA（DAMPs），活性化した好中球が放出するNeutrophil Extracellular Traps（NETs）は，細胞外においては第XII因子を活性化する陰性荷電異物となり，内因系凝固反応を活性化する[17]。また，NETsの主要成分の1つであるヒストン（DAMPs）は，血小板を活性化する（図4）。このように，感染部位や組織損傷部位で血栓が形成されることは，局所で生じた混乱を中枢に持ち込ませないための意義があると考えられるが，同時に，血栓症としての病的側面も持ち合わせている[17]。急性冠症候群患者では，血栓中に細胞外HMGB1が検出され[18]，血清HMGB1値が予後予測因子となりうることが報告されている[19]。HMGB1高値が組織損傷の程度を反映した「結果」なのか，血栓症を惹起する「原因」となっているのか，更なる検討が必要である。

おわりに

PAMPs/DAMPsの概念は，免疫学の分野で提唱され，急性炎症の舞台で研究が進み，近年は慢性炎症との関連が注目を集めている。診断マーカーとしての意義を越え，PAMPs/DAMPsを制御することで炎症性疾患を治療しようとする試みが進められている。

文　献

1) Matzinger P. The danger model: a renewed sense of self. Science, 2002; 296: 301-305.
2) Kono H, Rock KL. How dying cells alert the immune system to danger. Nat Rev Immunol, 2008; 8: 279-289.
3) Rovere-Querini P, Capobianco A, Scaffidi P, *et al*. HMGB1 is an endogenous immune adjuvant released by necrotic cells. EMBO Rep, 2004; 5: 825-830.
4) Zhang Q, Raoof M, Chen Y, *et al*. Circulating mitochondrial DAMPs cause inflammatory responses to injury. Nature, 2010; 464: 104-107.
5) Scaffidi P, Misteli T, Bianchi ME. Release of chromatin protein HMGB1 by necrotic cells triggers inflammation. Nature, 2002; 418: 191-195.
6) McDonald B, Pittman K, Menezes GB, *et al*. Intravascular danger signals guide neutrophils to sites of sterile inflammation. Science, 2010; 330: 362-366.
7) Palumbo R, Sampaolesi M, De Marchis F, *et al*. Extracellular HMGB1, a signal of tissue damage, induces mesoangioblast migration and proliferation. J Cell Biol, 2004; 164: 441-449.
8) Tschopp J, Schroder K. NLRP3 inflammasome activation: The convergence of multiple signalling pathways on ROS production? Nat Rev Immunol, 2010; 10: 210-215.
9) Sander LE, Davis MJ, Boekschoten MV, *et al*. Detection of prokaryotic mRNA signifies microbial viability and promotes immunity. Nature, 2011; 474: 385-389.
10) Medzhitov R. Origin and physiological roles of inflammation. Nature, 2008; 454: 428-435.
11) Zhou R, Tardivel A, Thorens B, *et al*. Thioredoxin-interacting protein links oxidative stress to inflammasome activation. Nat Immunol, 2010; 11: 136-140.
12) Duewell P, Kono H, Rayner KJ, *et al*. NLRP3 inflammasomes are required for atherogenesis and activated by cholesterol crystals. Nature, 2010; 464: 1357-1361.
13) Li L, Chen L, Hu L, *et al*. Nuclear factor high-mobility group box1 mediating the activation of Toll-like receptor 4 signaling in hepatocytes in the early stage of nonalcoholic fatty liver disease in mice. Hepatology, 2011; 54: 1620-1630.
14) Shrestha C, Ito T, Kawahara KI, *et al*. Saturated fatty acid palmitate induces extracellular release of histone H3: A possible mechanistic basis for high-fat diet-induced inflammation and thrombosis. Biochem Biophys Res Commun, 2013.
15) Ito T, Kawahara K, Nakamura T, *et al*. High-mobility group box 1 protein promotes development of microvascular thrombosis in rats. J Thromb Haemost, 2007; 5: 109-116.
16) Furlan-Freguia C, Marchese P, Gruber A, *et al*. P2X7 receptor signaling contributes to tissue factor-dependent thrombosis in mice. J Clin Invest, 2011; 121: 2932-2944.
17) Engelmann B, Massberg S. Thrombosis as an intravascular effector of innate immunity. Nat Rev Immunol, 2013; 13: 34-45.
18) Yamashita A, Nishihira K, Matsuura Y, *et al*. Paucity of CD34-positive cells and increased expression of high-mobility group box 1 in coronary thrombus with type 2 diabetes mellitus. Atherosclerosis, 2012; 224: 511-514.
19) Hashimoto T, Ishii J, Kitagawa F, *et al*. Circulating high-mobility group box 1 and cardiovascular mortality in unstable angina and non-ST-segment elevation myocardial infarction. Atherosclerosis, 2012; 221: 490-495.

Biochemical and Biophysical Research Communications 437 (2013) 573–578

Contents lists available at SciVerse ScienceDirect

Biochemical and Biophysical Research Communications

journal homepage: www.elsevier.com/locate/ybbrc

Saturated fatty acid palmitate induces extracellular release of histone H3: A possible mechanistic basis for high-fat diet-induced inflammation and thrombosis

Chandan Shrestha [a,b], Takashi Ito [a], Ko-ichi Kawahara [c], Binita Shrestha [b], Munekazu Yamakuchi [b], Teruto Hashiguchi [b], Ikuro Maruyama [a,*]

[a] Department of Systems Biology in Thromboregulation, Kagoshima University Graduate School of Medical and Dental Sciences, Kagoshima, Japan
[b] Department of Laboratory and Vascular Medicine, Kagoshima University Graduate School of Medical and Dental Sciences, Kagoshima, Japan
[c] Department of Biomedical Engineering, Osaka Institute of Technology, Osaka, Japan

ARTICLE INFO

Article history:
Received 18 June 2013
Available online 10 July 2013

Keywords:
High-fat diet
Palmitate
ROS
JNK
Histone H3
Inflammation

ABSTRACT

Chronic low-grade inflammation is a key contributor to high-fat diet (HFD)-related diseases, such as type 2 diabetes, non-alcoholic steatohepatitis, and atherosclerosis. The inflammation is characterized by infiltration of inflammatory cells, particularly macrophages, into obese adipose tissue. However, the molecular mechanisms by which a HFD induces low-grade inflammation are poorly understood. Here, we show that histone H3, a major protein component of chromatin, is released into the extracellular space when mice are fed a HFD or macrophages are stimulated with the saturated fatty acid palmitate. In a murine macrophage cell line, RAW 264.7, palmitate activated reactive oxygen species (ROS) production and JNK signaling. Inhibitors of these pathways dampened palmitate-induced histone H3 release, suggesting that the extracellular release of histone H3 was mediated, in part, through ROS and JNK signaling. Extracellular histone activated endothelial cells toexpress the adhesion molecules ICAM-1 and VCAM-1 and the procoagulant molecule tissue factor, which are known to contribute to inflammatory cell recruitment and thrombosis. These results suggest the possible contribution of extracellular histone to the pathogenesis of HFD-induced inflammation and thrombosis.

1. Introduction

Overweight status and obesity are risk factors for the development of insulin resistance, type 2 diabetes mellitus, atherosclerosis, and fatty liver diseases [1], which are generally caused by increased consumption of high-fat foods with reduced physical activity [2]. Beside these metabolic disorders, obesity is also associated with prothrombotic complication with excess production of tissue factor and plasminogen activator inhibitor-1 [3,4]. Chronic low-grade inflammation is a key contributor to the initiation and development of obesity-related diseases [5], and is characterized by increased secretion of proinflammatory cytokines (TNF-α, IL-6) and decreased secretion of anti-inflammatory cytokines (adiponectin, IL-10) [6,7]. Macrophages are one of the major sources of the inflammatory responses [8], which are associated with high cell infiltration of expanding adipose tissue in obese individuals [7]. In addition to increased macrophage recruitment to adipose tissue, obesity polarizes anti-inflammatory macrophages (M2; alternatively activated macrophages) to proinflammatory macrophages (M1; classically activated macrophages) [9].

Free fatty acid (FFA) levels are elevated in obese subjects through release from enlarged adipose tissue or reduced clearance [10]. FFA promotes inflammatory response signaling through Toll-like receptor (TLR) 4 and activates NF-κB and/or JNK signaling pathways that lead to insulin resistance, hepatic steatosis, and atherosclerosis [6,11–13]. Attenuation of these inflammatory responses, by targeting NF-κB or JNK or neutralizing TNF-α and IL-1β, improves insulin resistance and fatty liver diseases [14–16]. In addition to activation of TLR4, it has been reported that FFA activates NLRP3 inflammasomes, leading to activation of caspase 1 and secretion of IL-1β and IL-18 [16].

Although chronic low-grade inflammation plays a role in obesity-related complications [1,5], little is known about the molecular mechanism underlying its occurrence during HFD intake. A recent study showed that histones, which are nuclear proteins, function as endogenous danger signals or alarmins when they are released into the extracellular space during ischemia-reperfusion injury [17]. Extracellular histones can bind to different immune receptors, TLR2, TLR4, and TLR9, and contribute to leukocytosis, endothelial

* Corresponding author. Address: Department of Systems Biology in Thromboregulation, Kagoshima University Graduate School of Medical and Dental Sciences, 8-35-1 Sakuragaoka, Kagoshima 890-8544, Japan. Fax: +81 99 275 6463.
E-mail address: rinken@m3.kufm.kagoshima-u.ac.jp (I. Maruyama).

0006-291X/$ - see front matter © 2013 Elsevier Inc. All rights reserved.
http://dx.doi.org/10.1016/j.bbrc.2013.06.117

dysfunctions, organ failure, and even death [17–20]. In the present study, we show that HFD feeding or FFA treatment induces an active secretion of histone H3 into the extracellular space. This secretion is mediated, in part, through reactive oxygen species (ROS) production and the JNK signaling pathway. The extracellular histone then activates endothelial cells to express adhesion molecules, intracellular adhesion molecule-1 (ICAM-1) and vascular cell adhesion molecule-1 (VCAM-1), and a procoagulant molecule, tissue factor. These findings suggest the possible contribution of extracellular histone to the pathogenesis of HFD-induced inflammation and thrombosis.

2. Materials and methods

2.1. Reagents

Sodium palmitate (P9767), FFA-free BSA (A6003), N-acetyl cysteine (NAC) (A9165), Bay-11 7082 and oleate (07501G) were obtained from Sigma–Aldrich (St Louis, MO, USA). SP600125 (FA-005) was purchased from SABioscience (Valencia, CA, Spain). SB203580 (559389) and U0126 (662005) were obtained from Calbiochem (Billerica, MA, USA). Anti-histone H3 antibodies, sc-8654 and ab1791, were purchased from Santa Cruz Biotechnology (Dallas, TX, USA) and Abcam (Cambridge, MA, UK), respectively. Antibodies against p-SAPK/JNK, p-p42/44, p-p38, and p-p65 were purchased from Cell Signaling Technology (Beverly, MA, Canada).

2.2. Palmitate/BSA complex solution preparation

The palmitate/BSA solution was prepared as described previously [21] with slight modifications. Briefly, 100 mM palmitate solution was solubilized in 50% ethanol and then conjugated with 5% FFA-free BSA to achieve a final palmitate concentration of 5 mM. The conjugation was performed to increase the solubility of palmitate. The corresponding BSA solution with ethanol was used as a control. The solutions were prepared on the same day of the experiments.

2.3. Cell culture and treatment

A murine macrophage cell line, RAW 264.7, was obtained from the American Type Culture Collection (Manassas, VA, USA). The cells were cultured in RPMI-1640 medium (Sigma Chemical Co., St. Louis, MO, USA) supplemented with 10% FBS (Hyclone, Logan, UT, USA), 100 U/ml penicillin–streptomycin, and 5 mg/L amphotericin. The cells were maintained at 37 °C under 5% CO_2. The cells were starved for 2 h in serum-free medium and then stimulated with palmitate/BSA (Pa–BSA) or BSA solution as indicated. Pretreatments with different inhibitors were carried out 1 h before cell stimulation.

2.4. Sample preparation for histone H3

The histone H3 levels in culture supernatants were analyzed by Western blotting as described previously [22]. Briefly, 1.6 ml of supernatant was incubated with heparin-Sepharose 6B beads (GE Healthcare Bio-Science, Piscataway, NJ) at 4 °C overnight, washed with PBS, and mixed with sample buffer for SDS–PAGE.

2.5. Western blotting

Cell lysates or prepared samples were separated by 10–15% SDS–PAGE, transferred to nitrocellulose membranes, blocked with 5% nonfat dry milk, and incubated with specific primary antibodies against histone H3 (1:500; Santa Cruz Biotechnology), p-SAPK/JNK (1:1000), p-p42/p44 (1:1000), p-p38 (1:1000), p-p65 (1:1000) and β-actin (1:1000; Santa Cruz Biotechnology) at 4 °C overnight. The membranes were then incubated with horseradish peroxidase-conjugated secondary antibodies (1:3000; MP Biomedicals, L.L.C, Irvine, CA, USA) followed by detection with an ECL detection system (Thermo Scientific, Waltham, MA, USA). The band intensities were measured using ImageJ 1.46 software (National Institutes of Health, Bethesda, MD, USA).

2.6. Immunocytochemistry

RAW 264.7 cells plated on four-chamber culture slides for 16 h were fixed with 2% paraformaldehyde, permeabilized with a mixture of ethanol and acetone (2:1) at −20 °C for 5 min, and blocked with 1% BSA in PBS containing 0.1% Triton X-100. The cells were then sequentially incubated with an anti-histone H3 antibody (1:250; Abcam) for 24 h at 4 °C, and an Alexa Fluor 488-labeled goat anti-rabbit secondary antibody (A11070; Life Technologies, Carlsbad, CA, USA) for 1 h. The nuclei were stained with DAPI. The stained cells were visualized and photographed under a confocal microscope (LSM700; Carl Zeiss, Oberkochen, Germany).

2.7. Immunohistochemical staining

Immunohistochemical staining of histone H3 was performed as described previously [23] with slight modifications. Briefly, epididymal adipose tissue samples from male C57BL/6J mice fed a normal chow diet (crude fat: 4.6%, CLEA Japan Inc., Tokyo, Japan) or HFD-60 (crude fat: 35%, Oriental Yeast Co., Tokyo, Japan) for 12 weeks, were fixed in 10% formaldehyde neutral buffer, paraffin-embedded, and sectioned. The tissue sections were deparaffinized and rehydrated. Endogenous peroxidase activity was blocked in the presence of 0.3% hydrogen peroxide in methanol for 15 min. After antigen retrieval using an antigen-unmasking solution (Vector Laboratories Inc., Burlingame, CA, USA), the sections were blocked with 1% BSA in PBS containing 0.01% Tween 20 for 1 h. Subsequently, the sections were incubated with a rabbit anti-histone H3 antibody (1:800; Abcam) for 30 min at room temperature, followed by incubation with a secondary antibody for 30 min using a Histofine Simple Stain Mouse MAX-PO Kit (Nichirei Co., Tokyo, Japan). Finally, the sections were stained with DAB and counterstained with hematoxylin. Photographs were taken using a Zeiss Axiophot microscope (Carl Zeiss, Oberkochen, Germany).

2.8. ROS measurement

Intracellular ROS production was detected using the fluorescent probe H_2DCFDA (C400; Life Technologies) as described previously [24]. Briefly, RAW 264.7 cells treated with palmitate for 8 h were washed and incubated with 10 μM H_2DCFDA for 45 min at 37 °C. The fluorescence signals were analyzed using an Epics XL flow cytometer (Beckman Coulter, Miami, FL, USA).

2.9. Total RNA isolation and quantitative real-time RT-PCR

Human umbilical vein endothelial cells (HUVECs) were treated with purified unfractionated calf thymus histone (Sigma–Aldrich, St. Louis, MO, USA) at concentrations of 0, 10 and 20 μg/ml for 4 h. Total RNA was extracted from HUVECs using an RNAqueous Total RNA Isolation Kit (Ambion, Austin, TX, USA) according to the manufacturer's protocol, and reverse-transcribed to cDNA. The mRNA expression levels of inflammatory genes were assessed with specific primers (Assay IDs: tissue factor, Hs01076029_m1; ICAM-1, Hs00164932_m1; VCAM-1, Hs003655486_m1; TLR 2, Hs00610101_m1 and TLR 4, Hs00370853_m1) as described previously [23]. Expression levels were calculated as the ratio of mRNA

level for a given gene relative to the mRNA level for glyceraldehyde-3-phosphate dehydrogenase (GAPDH) in the same cDNA sample.

2.10. Flow cytometric assay of tissue factor, ICAM-1 and VCAM-1

The cell surface expressions of tissue factor protein, ICAM-1 and VCAM-1 protein were assessed by flow cytometry as described previously [25] using fluorescein isothiocyanate (FITC)-conjugated monoclonal antibodies against human tissue factor (Sekisui Diagnostics), ICAM-1 (Beckman Coulter, Marseille, France) and VCAM-1 (BD Pharmingen).

2.11. Cell viability assay

Cell viability was assessed by MTT assays as described previously [22]. Briefly, 5×10^5 cells in 24-well plates were treated with different concentrations of palmitate (0–200 μM) for 16 h. The cells were then incubated with MTT solution for 3 h. The formazan product was solubilized in dimethyl sulfoxide, and the absorbances were measured at a wavelength of 570 nm with a reference wavelength of 630 nm.

2.12. Statistical analysis

All results are expressed as means ± SEM, and were statistically analyzed by one-way ANOVA or a *t*-test using Prism software. Values of $P < 0.05$ were considered statistically significant.

3. Results

3.1. Extranuclear release of histone H3 in HFD-fed mice

Histones are found in the nucleus of resting cells where they regulate transcription and are involved in chromatin remodeling [18,19]. Consistent with this, histone H3 was mainly localized in the cell nuclei in mice fed the normal chow (Fig. 1A, left panel). However, extranuclear histone H3 was increased in mice fed the HFD (Fig. 1A, right panel). An increase in extranuclear histone H3 was also observed in murine macrophage cell line RAW 264.7 cells treated with the saturated fatty acid palmitate (Fig. 1B). These results indicate that HFD feeding or saturated fatty acid treatment can induce translocation of histone H3 from the nucleus to the cytoplasm.

3.2. Saturated fatty acid palmitate induces extracellular release of histone H3 from RAW 264.7 cells

We treated RAW 264.7 cells with palmitate for time periods of 8–16 h and at increasing concentrations (0–200 μM) for 16 h. Palmitate induced extracellular release of histone H3 in 16 h (Fig. 2A) and in a dose-dependent manner (Fig. 2B). In contrast, the carrier protein BSA or unsaturated fatty acid oleate did not induce histone H3 release (Fig. 2C). The palmitate-induced histone H3 release was not caused by cell death (Fig. 2D), suggesting that active secretion, rather than passive leakage, may be involved in this process.

3.3. ROS and JNK signaling mediate palmitate-induced histone H3 release

Next, we examined the mechanism by which palmitate induces release of histone H3. In line with previous reports [16,26], palmitate induced ROS generation in RAW 264.7 cells (Fig. 3A). Treatment with NAC, a ROS inhibitor, attenuated ROS production (Fig. 3A) and inhibited palmitate-induced histone H3 release (Fig. 3B). These results indicate that palmitate-induced histone H3 release is mediated, in part, through ROS production. We further examined the signaling pathways for histone H3 release. As shown in Fig. 3C, palmitate increased the phosphorylation of p38, JNK, ERK1/2, and NF-κB p65. A selective inhibitor of JNK (SP600125) attenuated palmitate-induced histone H3 release,

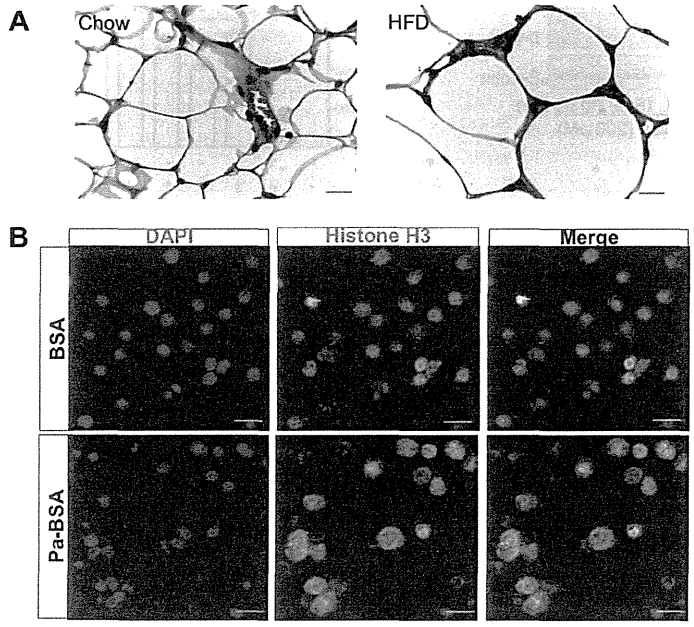

Fig. 1. Nuclear translocation of histone H3 *in vitro* and *in vivo*. (A) Representative photographs of immunostaining for histone H3 in adipose tissue from mice fed with a normal diet or HFD for 12 weeks. Original magnification: 40×; scale bar: 20 μm. (B) RAW 264.7 cells were plated on four-chamber culture slides and treated with 200 μM of BSA or palmitate/BSA (Pa-BSA) for 16 h. The cells were then immunostained for histone H3 and the nuclei were counterstained with DAPI. Original magnification: 20×; scale bar: 20 μm.

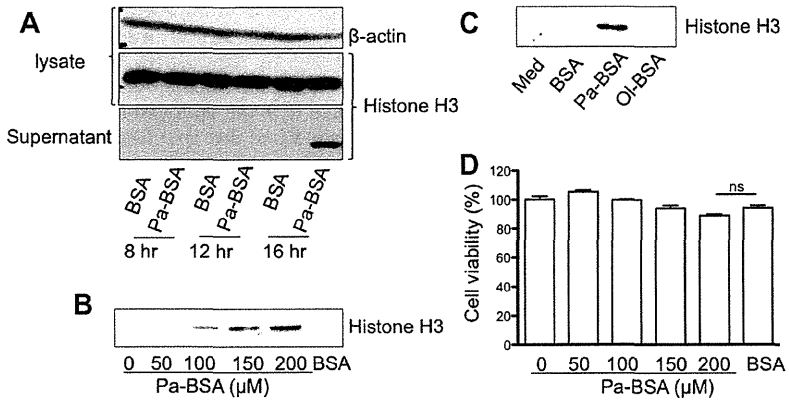

Fig. 2. Palmitate induces histone H3 release in time- and dose-dependent manners from RAW 264.7 cells. (A) RAW 264.7 cells were incubated with 200 μM of BSA or palmitate/BSA (Pa-BSA) for 8–16 h and histone H3 levels in supernatants and cell lysates were analyzed by Western blotting. (B) RAW 264.7 cells were incubated with increasing concentrations of Pa-BSA (0–200 μM) for 16 h and histone H3 levels in supernatants were analyzed by Western blotting. (C) RAW 264.7 cells were treated with 200 μM of BSA, Pa-BSA, or oleate/BSA (Ol-BSA) for 16 h, and histone H3 levels in supernatants were analyzed by Western blotting. (D) Cell viability was measured by MTT assays after 16 h of palmitate incubation.

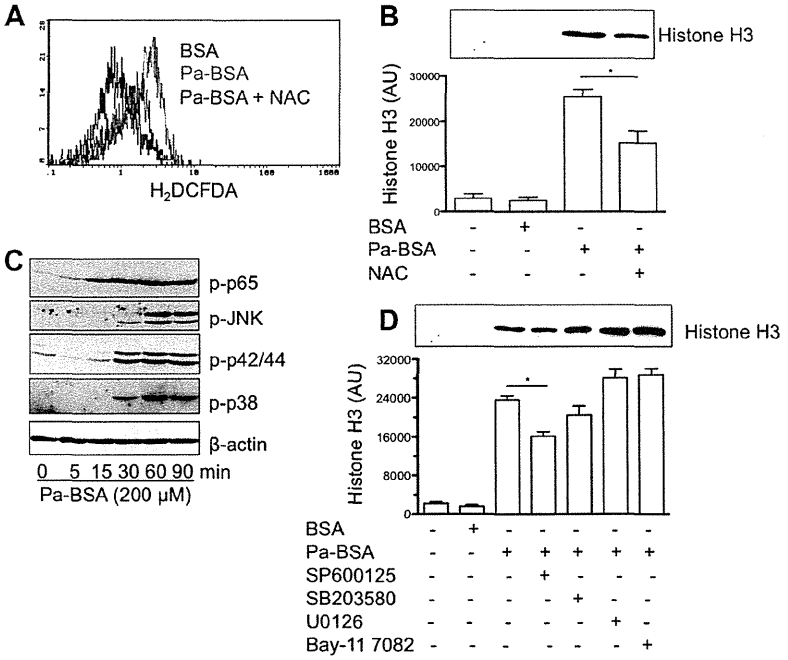

Fig. 3. Palmitate induces histone H3 through ROS and JNK signaling. (A) RAW 264.7 cells were treated with 200 μM of BSA or palmitate/BSA (Pa-BSA) for 8 h. Intracellular ROS production was measured using a fluorescent probe, H_2DCFDA. (B) RAW 264.7 cells were pretreated with NAC (5 mM) 1 h before palmitate stimulation. The histone H3 levels in the supernatants after 16 h were analyzed by Western blotting. (C) Immunoblotting for phospho-MAPKs and phospho-p65 in lysates of cells treated with palmitate (200 μM) for 0–90 min. (D) RAW 264.7 cells were pretreated with MAPK inhibitors (SB203580, SP600125, or U0126; 10 μM) and NF-κB inhibitors (10 μM) 1 h before cell stimulation. The histone H3 levels in the supernatants after 16 h were analyzed by Western blotting.

whereas a p38 inhibitor (SB203580), ERK1/2 inhibitor (U0126), and NF-κB inhibitor (Bay-11 7082) had no effects (Fig. 3B). These results indicate that palmitate-induced histone H3 release is mediated, in part, through the JNK signaling pathway.

3.4. Extracellular histone activates endothelial cells to express the adhesion molecules VCAM-1 and ICAM-1 and the procoagulant molecule tissue factor

Finally, we examined the effects of extracellular histone on the surrounding cells, including endothelial cells. Extracellular histone significantly increased the mRNA expressions of the adhesion molecules ICAM-1 and VCAM-1 and the procoagulant molecule tissue factor in endothelial cells in dose-dependent manners (Fig. 4A). Extracellular histone also increased the mRNA expression of TLR2, but not that of TLR4 (Fig. 4A), which were both reported to act as receptors for extracellular histones [18–20]. Furthermore, extracellularhistone induced the expression of ICAM-1, VCAM-1, and tissue factor proteins on the surface of endothelial cells (Fig. 4B). These results suggest a possible contribution of extracellular histones to the pathogenesis of HFD-induced inflammation and thrombosis.

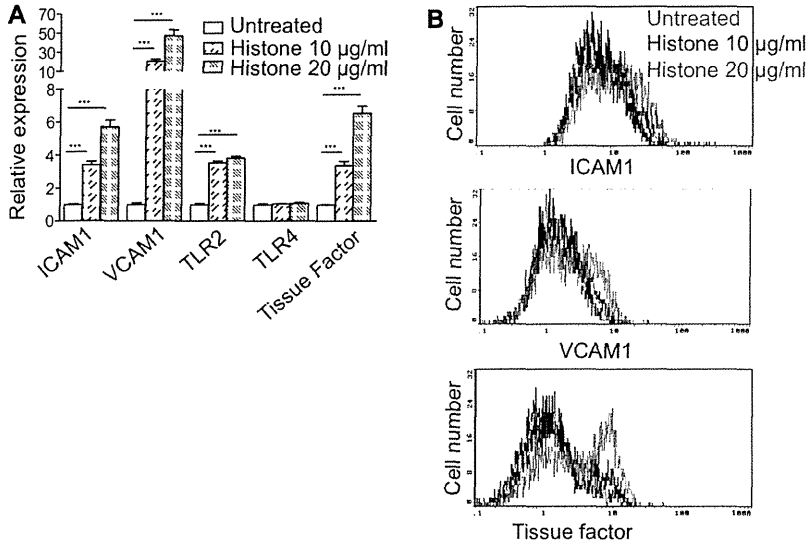

Fig. 4. Extracellular histone induces the expressions of the adhesion molecules ICAM-1 and VCAM-1 and the procoagulant molecule tissue factor in endothelial cells. (A) HUVECs were treated with histone at concentrations of 0, 10 and 20 μg/ml for 4 h, and the expressions of ICAM-1, VCAM-1, TLR2, TLR4 and tissue factor were analyzed by RT-PCR. (B) HUVECs were treated with histone for 6 h and measured for their surface expression of ICAM-1, VCAM-1 and tissue factor by flow cytometry.

4. Discussion

The present study has demonstrated that histone H3 is released into the extracellular space from macrophages treated with palmitate *in vitro* and adipose tissue in mice fed a HFD *in vivo*. The release of histone H3 is an active process in living cells, rather than passive leakage from dying cells. The extracellular histone then activates the endothelium to express cell adhesion molecules and procoagulant protein, tissue factor. These results suggest the possible contribution of extracellular histone to the pathogenesis of HFD-induced inflammation and thrombosis.

Histones are nuclear proteins that form hetero-octamers to wind up the double strands of DNA in nucleosomes and are involved in chromatin remodeling and gene transcription regulation [18,19]. Histones can be released into the extracellular space during sepsis, and the plasma concentration of histones can reach 70 μg/ml in the acute inflammatory condition [27]. In this study, we showed that histone H3 was also released into the extracellular space during chronic low-grade inflammation induced by HFD feeding or FFA treatment. Palmitate (C16:0) and oleate (C18:1) are most abundant saturated and unsaturated fatty acid, respectively, in HFD used in this study. Consistent with previous studies showing that palmitate induces expression of proinflammatory molecules [6,28,29], palmitate, but not oleate, induced histone H3 release in our *in vitro* study.

ROS are linked to multiple pathologies, such as cardiovascular diseases, diabetes, neurological disease, and cancer. The increased ROS levels during obesity deregulate the production of adipokines [30]. Consistent with previous data, we found that palmitate induced ROS generation from RAW 264.7 cells, and that treatment with NAC, a ROS inhibitor, inhibited the histone release. In addition to ROS, NF-κB and JNK, which are regulators of inflammation, have been reported to link obesity and metabolic diseases [12]. FFA activates both NF-κB and JNK signaling following activation of TLR4, leading to increased expressions of proinflammatory cytokines such as TNF-α and IL-6 [6]. Our results also demonstrated activation of NF-κB and MAPKs in time-dependent manners. Although palmitate activated these various pathways, incubation of the cells with ERK, p-38, and NF-κB inhibitors in presence of palmitate had no effects on the histone release. However, a JNK inhibitor inhibited the histone release. These results suggest that the JNK signaling pathway is involved in the histone release induced by palmitate.

A previous study showed that the JNK signaling pathway is activated by palmitate, and that inhibition of ROS reduces the activation of this signaling pathway and enhances insulin sensitivity in hepatocytes [26]. We treated cells with palmitate in the presence of NAC or a JNK inhibitor and measured the activation of JNK by Western blotting. The cells treated with the JNK inhibitor showed attenuated JNK activation, while NAC did not inhibit the JNK activation (data not shown). Our results show that the activation of JNK is not dependent on ROS and that both ROS and JNK activation partly contribute to the histone release induced by palmitate.

Finally, we performed *in vitro* experiments examining the effects of the extracellular histone. It has been reported that histones, which are released from dying cells during sepsis or inflammation, can activate TLR2/TLR4 and contribute to endothelial dysfunction [19]. ICAM-1 and VCAM-1 are upregulated during endothelial activation and involved in the interactions of inflammatory cells with the endothelium and the transmigration of these cells into adipose tissue [31]. We showed that the released histone induced the expressions of adhesion molecules ICAM-1 and VCAM-1 in endothelial cells and enhanced the expression of TLR2, but not TLR4. Besides these effects, the histone induced the expression of a procoagulant protein, tissue factor, from endothelial cells, which plays a crucial role in coagulation and thrombosis. A recent study showed that tissue factor promotes inflammation and diet-induced obesity through protease-activated receptor 2 (PAR2) [32].

In summary, our study has demonstrated that palmitate induces the release of histone H3 from activated macrophages, in part, through ROS generation and the JNK signaling pathway. The extracellular histone activates the endothelium and enhances proinflammatory and prothrombotic responses. Overall, we suggest that histones provide the cross-talk between obesity and inflammation. However, further studies are required to investigate the associations of histones with diet-induced obesity and inflammation.

Acknowledgments

We thank Nobue Uto (Department of Laboratory and Vascular Medicine), Tomoka Nagasato, and Mika Yamamoto (Department of Systems Biology in Thromboregulation) for their technical support.

Appendix A. Supplementary data

Supplementary data associated with this article can be found, in the online version, at http://dx.doi.org/10.1016/j.bbrc.2013.06.117.

References

[1] T.D. Kanneganti, V.D. Dixit, Immunological complications of obesity, Nat. Immunol. 13 (2012) 707–712.
[2] J.O. Hill, Understanding and addressing the epidemic of obesity: an energy balance perspective, Endocr. Rev. 27 (2006) 750–761.
[3] A. Singh, G.D. Foster, J. Gunawardana, T.A. McCoy, T. Nguyen, S. Vander Veur, E. Komaroff, A.K. Rao, Elevated circulating tissue factor procoagulant activity, factor VII, and plasminogen activator inhibitor-1 in childhood obesity: evidence of a procoagulant state, Br. J. Haematol. 158 (2012) 523–527.
[4] K.A. Darvall, R.C. Sam, S.H. Silverman, A.W. Bradbury, D.J. Adam, Obesity and thrombosis, Eur. J. Vasc. Endovasc. Surg. 33 (2007) 223–233.
[5] C.N. Lumeng, A.R. Saltiel, Inflammatory links between obesity and metabolic disease, J. Clin. Invest. 121 (2011) 2111–2117.
[6] H. Shi, M.V. Kokoeva, K. Inouye, I. Tzameli, H. Yin, J.S. Flier, TLR4 links innate immunity and fatty acid-induced insulin resistance, J. Clin. Invest. 116 (2006) 3015–3025.
[7] S.P. Weisberg, D. McCann, M. Desai, M. Rosenbaum, R.L. Leibel, A.W. Ferrante Jr., Obesity is associated with macrophage accumulation in adipose tissue, J. Clin. Invest. 112 (2003) 1796–1808.
[8] H. Xu, G.T. Barnes, Q. Yang, G. Tan, D. Yang, C.J. Chou, J. Sole, A. Nichols, J.S. Ross, L.A. Tartaglia, H. Chen, Chronic inflammation in fat plays a crucial role in the development of obesity-related insulin resistance, J. Clin. Invest. 112 (2003) 1821–1830.
[9] C.N. Lumeng, J.L. Bodzin, A.R. Saltiel, Obesity induces a phenotypic switch in adipose tissue macrophage polarization, J. Clin. Invest. 117 (2007) 175–184.
[10] G. Boden, Obesity and free fatty acids, Endocrinol. Metab. Clin. North Am. 37 (vii–ix) (2008) 635–646.
[11] J. Nigro, N. Osman, A.M. Dart, P.J. Little, Insulin resistance and atherosclerosis, Endocr. Rev. 27 (2006) 242–259.
[12] G. Solinas, M. Karin, JNK1 and IKKbeta: molecular links between obesity and metabolic dysfunction, FASEB J. 24 (2010) 2596–2611.
[13] L. Li, L. Chen, L. Hu, Y. Liu, H.Y. Sun, J. Tang, Y.J. Hou, Y.X. Chang, Q.Q. Tu, G.S. Feng, F. Shen, M.C. Wu, H.Y. Wang, Nuclear factor high-mobility group box1 mediating the activation of Toll-like receptor 4 signaling in hepatocytes in the early stage of nonalcoholic fatty liver disease in mice, Hepatology 54 (2011) 1620–1630.
[14] M.C. Arkan, A.L. Hevener, F.R. Greten, S. Maeda, Z.W. Li, J.M. Long, A. Wynshaw-Boris, G. Poli, J. Olefsky, M. Karin, IKK-beta links inflammation to obesity-induced insulin resistance, Nat. Med. 11 (2005) 191–198.
[15] M.S. Han, D.Y. Jung, C. Morel, S.A. Lakhani, J.K. Kim, R.A. Flavell, R.J. Davis, JNK expression by macrophages promotes obesity-induced insulin resistance and inflammation, Science 339 (2013) 218–222.
[16] H. Wen, D. Gris, Y. Lei, S. Jha, L. Zhang, M.T. Huang, W.J. Brickey, J.P. Ting, Fatty acid-induced NLRP3-ASC inflammasome activation interferes with insulin signaling, Nat. Immunol. 12 (2011) 408–415.
[17] H. Huang, J. Evankovich, W. Yan, G. Nace, L. Zhang, M. Ross, X. Liao, T. Billiar, J. Xu, C.T. Esmon, A. Tsung, Endogenous histones function as alarmins in sterile inflammatory liver injury through Toll-like receptor 9 in mice, Hepatology 54 (2011) 999–1008.
[18] R. Allam, C.R. Scherbaum, M.N. Darisipudi, S.R. Mulay, H. Hagele, J. Lichtnekert, J.H. Hagemann, K.V. Rupanagudi, M. Ryu, C. Schwarzenberger, B. Hohenstein, C. Hugo, B. Uhl, C.A. Reichel, F. Krombach, M. Monestier, H. Liapis, K. Moreth, L. Schaefer, H.J. Anders, Histones from dying renal cells aggravate kidney injury via TLR2 and TLR4, J. Am. Soc. Nephrol. 23 (2012) 1375–1388.
[19] F. Semeraro, C.T. Ammollo, J.H. Morrissey, G.L. Dale, P. Friese, N.L. Esmon, C.T. Esmon, Extracellular histones promote thrombin generation through platelet-dependent mechanisms: involvement of platelet TLR2 and TLR4, Blood 118 (2011) 1952–1961.
[20] J. Xu, X. Zhang, M. Monestier, N.L. Esmon, C.T. Esmon, Extracellular histones are mediators of death through TLR2 and TLR4 in mouse fatal liver injury, J. Immunol. 187 (2011) 2626–2631.
[21] S.P. Cousin, S.R. Hugl, C.E. Wrede, H. Kajio, M.G. Myers Jr., C.J. Rhodes, Free fatty acid-induced inhibition of glucose and insulin-like growth factor I-induced deoxyribonucleic acid synthesis in the pancreatic beta-cell line INS-1, Endocrinology 142 (2001) 229–240.
[22] Y. Nawa, K. Kawahara, S. Tancharoen, X. Meng, H. Sameshima, T. Ito, Y. Masuda, H. Imaizumi, T. Hashiguchi, I. Maruyama, Nucleophosmin may act as an alarmin: implications for severe sepsis, J. Leukoc. Biol. 86 (2009) 645–653.
[23] B. Shrestha, T. Hashiguchi, T. Ito, N. Miura, K. Takenouchi, Y. Oyama, K. Kawahara, S. Tancharoen, I.Y. Ki, N. Arimura, N. Yoshinaga, S. Noma, C. Shrestha, T. Nitanda, S. Kitajima, K. Arimura, M. Sato, T. Sakamoto, I. Maruyama, B cell-derived vascular endothelial growth factor A promotes lymphangiogenesis and high endothelial venule expansion in lymph nodes, J. Immunol. 184 (2010) 4819–4826.
[24] M.Y. Chang, C.Y. Han, T.N. Wight, A. Chait, Antioxidants inhibit the ability of lysophosphatidylcholine to regulate proteoglycan synthesis, Arterioscler. Thromb. Vasc. Biol. 26 (2006) 494–500.
[25] T. Ito, K. Kawahara, T. Nakamura, S. Yamada, K. Abeyama, T. Hashiguchi, I. Maruyama, High-mobility group box 1 protein promotes development of microvascular thrombosis in rats, J. Thromb. Haemost. 5 (2007) 109–116.
[26] S. Nakamura, T. Takamura, N. Matsuzawa-Nagata, H. Takayama, H. Misu, H. Noda, S. Nabemoto, S. Kurita, T. Ota, H. Ando, K. Miyamoto, S. Kaneko, Palmitate induces insulin resistance in H4IIEC3 hepatocytes through reactive oxygen species produced by mitochondria, J. Biol. Chem. 284 (2009) 14809–14818.
[27] J. Xu, X. Zhang, R. Pelayo, M. Monestier, C.T. Ammollo, F. Semeraro, F.B. Taylor, N.L. Esmon, F. Lupu, C.T. Esmon, Extracellular histones are major mediators of death in sepsis, Nat. Med. 15 (2009) 1318–1321.
[28] P.S. Laine, E.A. Schwartz, Y. Wang, W.Y. Zhang, S.K. Karnik, N. Musi, P.D. Reaven, Palmitic acid induces IP-10 expression in human macrophages via NF-kappaB activation, Biochem. Biophys. Res. Commun. 358 (2007) 150–155.
[29] J.Y. Lee, K.H. Sohn, S.H. Rhee, D. Hwang, Saturated fatty acids, but not unsaturated fatty acids, induce the expression of cyclooxygenase-2 mediated through Toll-like receptor 4, J. Biol. Chem. 276 (2001) 16683–16689.
[30] S. Furukawa, T. Fujita, M. Shimabukuro, M. Iwaki, Y. Yamada, Y. Nakajima, O. Nakayama, M. Makishima, M. Matsuda, I. Shimomura, Increased oxidative stress in obesity and its impact on metabolic syndrome, J. Clin. Invest. 114 (2004) 1752–1761.
[31] S.E. Shoelson, J. Lee, A.B. Goldfine, Inflammation and insulin resistance, J. Clin. Invest. 116 (2006) 1793–1801.
[32] L. Badeanlou, C. Furlan-Freguia, G. Yang, W. Ruf, F. Samad, Tissue factor-protease-activated receptor 2 signaling promotes diet-induced obesity and adipose inflammation, Nat. Med. 17 (2011) 1490–1497.

The images in Figures 2C, 3B and 3D are derived from one immunoblot film. The unprocessed, full-length blot is shown below. The addition of this Supplementary Figure will not affect the conclusions of Figures 2 or 3 at all.

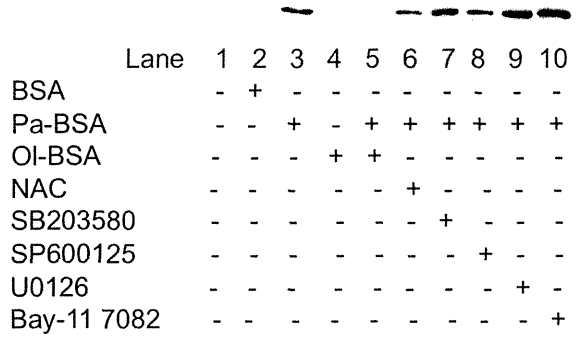

Lane	1	2	3	4	5	6	7	8	9	10
BSA	-	+	-	-	-	-	-	-	-	-
Pa-BSA	-	-	+	-	+	+	+	+	+	+
Ol-BSA	-	-	-	+	+	-	-	-	-	-
NAC	-	-	-	-	-	+	-	-	-	-
SB203580	-	-	-	-	-	-	+	-	-	-
SP600125	-	-	-	-	-	-	-	+	-	-
U0126	-	-	-	-	-	-	-	-	+	-
Bay-11 7082	-	-	-	-	-	-	-	-	-	+

Fig S. One set of experiments was divided into three parts (Fig. 2C, 3B and 3D) for a better understanding. RAW 264.7 cells were starved for 2 h in serum-free medium, pretreated with NAC, SB203580, SP600125, U0126, or Bay-11 7082 for 1 h, and stimulated with BSA, palmitate/BSA (Pa-BSA), or oleate/BSA (Ol-BSA). The histone H3 levels in the supernatants after 16 h were analyzed by western blotting. All the treatments above were performed simultaneously. Lanes 1, 2, 3, and 4 are used in Fig 2C, lanes 1, 2, 3, and 6 are used in Fig 3B, and lanes 1, 2, 3, 7, 8, 9, and 10 are used in Fig 3D.

Preventive effects of *Morus alba L.* anthocyanins on diabetes in Zucker diabetic fatty rats

ARIYA SARIKAPHUTI[1], THAMTHIWAT NARARATWANCHAI[1], TERUTO HASHIGUCHI[2], TAKASHI ITO[3], SITA THAWORANUNTA[4], KIYOSHI KIKUCHI[5], YOKO OYAMA[2], IKURO MARUYAMA[3] and SALUNYA TANCHAROEN[6]

[1]School of Anti-Aging and Regenerative Medicine, Mae Fah Luang University, Bangkok 10110, Thailand; Departments of [2]Laboratory and Vascular Medicine, and [3]Systems Biology in Thromboregulation, Kagoshima University Graduate School of Medical and Dental Sciences, Kagoshima 890-8520, Japan; [4]Department of Prosthodontics, Faculty of Dentistry, Mahidol University, Bangkok 10400, Thailand; [5]Departments of Physiology and Neurosurgery, Kurume University School of Medicine, Fukuoka 830-0011, Japan; [6]Department of Pharmacology, Faculty of Dentistry, Mahidol University, Bangkok 10400, Thailand

Received March 13, 2013; Accepted June 14, 2013

DOI: 10.3892/etm.2013.1203

Abstract. The mulberry plant (*Morus alba L.*) contains abundant anthocyanins (ANCs), which are natural antioxidants. The aim of this study was to determine the ANC composition of Thai *Morus alba* L. fruits and to assess the effect of an ANC extract on blood glucose and insulin levels in male leptin receptor-deficient Zucker diabetic fatty (ZDF) rats. The major components of the ANC extract were identified by high-performance liquid chromatography-electrospray ionization-mass spectrometry. ZDF and lean rats were treated with 125 or 250 mg ANCs/kg body weight, or 1% carboxymethylcellulose (CMC) twice daily for 5 weeks. Neither ANC dose had an effect on body weight. Following 5 weeks of treatment, glucose levels were observed to increase from 105.5±8.7 to 396.25±21 mg/dl ($P<0.0001$) in the CMC-treated ZDF rats; however, the glucose levels were significantly lower in the rats treated with 125 or 250 mg/kg ANCs (228.25±45 and 131.75±10 mg/dl, respectively; $P<0.001$ versus CMC). The administration of 250 mg/kg ANCs normalized glucose levels in the ZDF rats towards those of the lean littermates. Insulin levels were decreased significantly in the ZDF rats treated with CMC or 125 mg/kg ANCs ($P<0.0001$), but not in the rats treated with 250 mg/kg ANCs. Histologically, 250 mg/kg ANCs was observed to prevent islet degeneration compared with the islets in CMC-treated rats. This study, demonstrated that ANCs extracted from *Morus alba L.* were well tolerated and exhibited effective anti-diabetic properties in ZDF rats. ANCs represent a promising class of therapeutic compounds that may be useful in the prevention of type 2 diabetes.

Correspondence to: Dr Salunya Tancharoen, Department of Pharmacology, Faculty of Dentistry, Mahidol University, 6 Yothe Road, Rajthevee, Bangkok 10400, Thailand
E-mail: salunya.tan@mahidol.ac.th

Key words: *Morus alba L.*, anthocyanins, type 2 diabetes, disease prevention

Introduction

Type 2 diabetes is preceded by the inability of β-cells to secrete sufficient insulin to overcome insulin resistance or reduced insulin sensitivity, combined with reduced insulin secretion. Degeneration of the islets of Langerhans with β-cell loss is secondary to insulin resistance and is regarded as the pathophysiology of type 2 diabetes (1). Oral hypoglycemic agents directly stimulate insulin release from β-cells to overcome insulin resistance and normalize blood glucose levels. However, these drugs may induce certain adverse effects, such as hypoglycemia (2,3). The consumption of anthocyanins (ANCs) has been suggested to be correlated with a reduced risk of degenerative diseases, such as atherosclerosis (4), cardiovascular diseases (5), cancer (6) and diabetes (7). ANCs extracted from *Calendula officinalis* fruits have been reported to enhance insulin release from pancreatic β-cells *in vitro* (8). Mulberry leaves and fruits have been used in the treatment of numerous diseases (9-12). The mulberry fruit (*Morus alba L.*, family Moraceae) contains abundant ANCs, which scavenge reactive oxygen species (13), have anti-obesity effects and inhibit low-density lipoprotein oxidation (14). The predominant ANCs in mulberry, cyanidin 3-rutinoside and cyanidin 3-glucoside, have been demonstrated to dose-dependently inhibit the migration and invasion of highly metastatic A549 human lung carcinoma cells (15). Furthermore, it was recently demonstrated that the cyanidin 3-O-β-D-glucopyranoside fraction from mulberry fruit protected against bladder dysfunction in streptozotocin-induced diabetic rats (16). However, it has not yet been elucidated whether the ANCs in mulberry are able to significantly lower blood glucose levels and whether they may be useful in the treatment of the pathogenesis of type 2 diabetes.

The evolution of diabetes in male leptin receptor-deficient Zucker diabetic fatty (ZDF) rats (ZDF/CrlCrlj) has resulted in it becoming a popular model for preclinical studies of type 2 diabetes, due to the fact that these rats exhibit disrupted islet architecture, β-cell degranulation and increased β-cell death (17,18). Therefore, ZDF male rats were used as a rodent model of type 2 diabetes in the present study. It was hypothesized that the consumption of an ANC extract from Thai *Morus alba L.* fruits was likely to result in glucose-lowering effects and enhanced insulin secretion. The purpose of this study was to determine the ANC composition of Thai *Morus alba L.* fruits, and to assess the effect of an ANC extract on the blood glucose and insulin levels in ZDF rats. To the best of our knowledge, the present study has demonstrated for the first time that ANCs extracted from Thai *Morus alba L.* have significant anti-diabetic activity. Furthermore, the ANC extract appeared to prevent the development of pathogenic lesions in diabetic islets by suppressing islet degeneration.

Material and methods

Plant material and extraction. Mulberry fruits were obtained from Kamnan Jul Farm, Petchaboon Province, Thailand. The fruit was extracted in ethanol-water (50/50, v/v%), prior to the extract being filtered through a Buchner funnel and filter paper (Chmlab, Barcelona, Spain) and transferred to a 100 ml flask. The extract was then collected and condensed at 40˚C using a Büchi B-490 rotary evaporator (Büchi Labortechnik AG, Flawil, Switzerland) under a vacuum and lyophilized with a freeze-dryer (Labconco Corp., Kansas City, MO, USA).

Isolation and purification of mulberry ANCs. A C18 Sep-Pak cartridge (Waters Corp., Milford, MO, US) was activated for 30 min with distilled water and high-performance liquid chromatography (HPLC)-grade methanol (Merck KGaA, Darmstadt, Germany). The ANC extract was then loaded onto the column. Following successive washes with five volumes of distilled water (acidified with 0.01% HCl) and ethyl acetate (Fisher Scientific UK Ltd., Loughborough, UK), the ANCs were eluted with methanol containing 0.01% HCl. The ANC solution was then collected and condensed at 40˚C using a Büchi B-490 rotary evaporator under vacuum.

HPLC-electrospray ionization (ESI)-mass spectrometry (MS). ANCs in the partially purified extracts were separated and quantified by reverse-phase HPLC using a Hypersil™ Gold C18 column (inner diameter, 5 μm; 4.6x250 mm; Thermo Fisher Scientific Inc., Salt Lake City, IL, USA). The column was eluted with a mobile phase consisting of water, 3.75% formic acid (VWR International, Ltd., Lutterworth, UK) and 15% methanol at a flow rate of 1 ml/min. The separated ANCs were detected and measured at 530 nm, and were identified based on the retention times and ultraviolet (UV)-visible (Vis) wavelength spectra of pure authentic standards (cyanidin 3-O-glucoside, cyanidin 3-rutinoside, pelargonidin 3-glucoside and pelargonidin 3-rutinoside; Sigma, St. Louis, MO, USA). The identity of each peak was verified by LC-MS (Agilent 1100; Agilent Technologies, Santa Clara, CA, USA) using ESI and operating in a single quadrupole mode. The instrument was scanned over the *m/z* range of 200-1,500 in the ESI positive ion mode. The LC-MS was eluted with acetonitrile (Fisher Scientific UK Ltd.) and 0.5% ammonium hydroxide (90:10, v/v%).

Quantification of ANCs by UV-Vis spectroscopy. The ANCs were quantified by UV-Vis spectroscopy, as previously described (19). The model reaction solution was diluted with 0.01% HCl in distilled water and the absorbance at 510 nm was compared with that of known standard solutions using a Genesys 10 UV spectrophotometer (Thermo Spectronic, Rochester, NY, USA).

Determination of total phenolic content. The total phenolic content was determined using the Folin-Ciocalteau reagent (FCR), as previously described (20), with minor modifications. Briefly, 2.5 ml ethanolic mulberry extract was mixed with 0.5 ml FCR (Sigma) and 1.0 ml 20 g/100 g solution of sodium carbonate. The mixture was then incubated for 2 h in the dark at 25˚C. The absorbance of the mixture was measured at 765 nm using a UV-Vis Genesys 10 UV spectrophotometer (Thermo Spectronic). A standard curve was plotted using gallic acid (0.07-10 mg/ml in methanol; Sigma) as a standard. The total phenolic content was expressed as gallic acid equivalents (GAEmM/Gfw). The assay was carried out in triplicate and the mean value was recorded.

Determination of ferric-reducing antioxidant power (FRAP). FRAP was measured as previously described (21). Briefly, FRAP reagent, which consisted of 0.3 M acetate buffer (pH 3.6), 10 mM 2,4,6-tris(2-pyridyl)-s-triazine (TPTZ) (Fluka, Buchs, Switzerland) in 40 mM HCl and 20 mM $FeCl_3.6H_2O$ at a ratio of 10:1:1 (v/v/v) was freshly prepared prior to each measurement. Following this, 200 μl mulberry extract was mixed with 1.3 ml FRAP reagent and incubated for 30 min at 37˚C. The absorption was measured at 595 nm using an Epoch spectrophotometer (Bio-Tek Instruments, Inc. Winooski, VT, USA) with the Gen5 Data Analysis Software interface. Aqueous or methanol solutions containing known Fe(II) concentrations were used to calibrate the FRAP assay. FRAP values, expressed as mmol of Fe(II) equivalents (FeFmM/gFW), were determined by comparing the change in the absorption of the test mixture with that of the Fe(II) standards. The assay was carried out in triplicate and the mean value was recorded.

Evaluation of the anti-diabetic effects of ANCs in ZDF rats. Five-week-old male ZDF ($Lepr^{fa}$/CrlCrlj) and age-matched lean rats ($Lepr^{fa}/\pm$) were used in this study. All rats were ordered as bred from Charles River Laboratories International (Wilmington, MA, USA). All animal studies were conducted according to the National Institutes of Health Guidelines for the Care and Use of Animals, and were reviewed and approved by the Committee on Animal Experimentation of Kagoshima University (Kagoshima, Japan). The rats were kept under pathogen-free conditions with a 12-h light-dark cycle (lights on at 07:00) at 22±1˚C.

The ZDF and lean rats were treated with 125 or 250 mg ANCs/body weight dissolved in 1% CMC (Sigma) in distilled water by gavage, twice daily. The control groups received 1% carboxymethylcellulose (CMC) in distilled water alone.

Following the allocation of the rats to each experimental group, the rats were left to acclimatize and were fed a control diet for 1 week. Food was then withheld for 24 h and tail vein blood samples were collected subsequent to cutting the tip of the tail with a scalpel. The blood samples were centrifuged, and the plasma was stored at -20°C until assay. Blood glucose levels were monitored every week using a glucose meter (Accu-Chek® Active; Roche Diagnostics). Following 5 weeks of treatment with ANCs or CMC, the rats were sacrificed by heart puncture using sterile needles and syringes under anesthesia with diethyl ether, and blood was collected. Plasma insulin levels were measured using an enzyme immunoassay (Cayman Chemical Co., Ann Arbor, MI, USA). All experiments were performed using conscious unrestrained rats.

Following the sacrifice of the rats, the pancreas was perfused with physiological saline and rapidly excised. The tissue samples were maintained in 10% neutral-buffered formalin, dehydrated in a graded ethanol series, cleared in xylene and embedded in paraffin wax. Sections (4 μm thick) were stained with hematoxylin and eosin (H&E). For histological analysis, the tissue sections were photographed using a high-resolution color digital camera mounted on an Olympus BX51 microscope (Olympus, Tokyo, Japan), and the images were transferred to a computer. Four sections were examined from each animal in each treatment group.

Cell culture and treatment. Murine macrophage-like cells (RAW 264.7) and rat renal tubular epithelial cells (NRK-52E) were obtained from the American Type Culture Collection (Manassas, VA, USA). RAW 264.7 cells were maintained in RPMI-1640 medium (Gibco BRL, Grand Island, NY, USA) supplemented with 10% fetal bovine serum and 2 mmol/l glutamine (Hyclone, Logan, UT, USA). NRK-52E cells were grown in Dulbecco's modified Eagle's medium (DMEM; Gibco BRL) containing 7% (v/v%) fetal bovine serum and 2 mmol/l glutamine (Hyclone). RAW 264.7 cells ($3.5x10^4$ cells/well) and NRK-52E cells ($4x10^4$ cells/well) were cultured in serum-free Opti-MEM® I medium (Gibco BRL) and serum-free DMEM, respectively, prior to stimulation with various concentrations (0, 2, 10, 30, 50 or 100 μg/ml) of mulberry extract for 24 h.

Methylthiazolyl-diphenyl-tetrazolium bromide (MTT) assay. Cell viability was assessed using a modified MTT assay. Briefly, following the exposure of the cells to the specified concentration of mulberry extract for 48 h, MTT solution was added to each well of the six-well plate. Three hours subsequently, dimethyl sulfoxide (DMSO) was added and the plate was incubated for 24 h at 37°C. Absorbance was measured at 570 nm using an automatic microplate reader (ImmunoMini NJ-2300; InterMed, Tokyo, Japan).

Statistical analysis. Data were analyzed using SPSS statistical software version 3.0 (SPSS, Inc., Chicago, IL, USA). Data are shown as the mean ± standard deviation. The significance of the differences between two groups was assessed using the Student's t-test, and differences between multiple groups were assessed by one-way analysis of variance (ANOVA) followed by the Scheffé's multiple range test. Values of $P<0.05$ were considered to indicate a statistically significant difference.

Results

Analysis of mulberry ANCs. The ANC composition of mulberry fruit was determined by HPLC-ESI-MS. The ANC extract was purified using a C-18 Sep-Pak cartridge, and the resulting chromatogram, at 520 nm, is shown in Fig. 1. The chromatogram contained four peaks within the retention time of 31-38 min, indicating the presence of four different ANCs in mulberry fruit (Table I). Peak 1, with a retention time of 31.3 min, M+ at *m/z* 449.1 and a fragment ion at *m/z* 287.0, was identified as cyanidin 3-O-glucoside (51.4%). Peak 2, with a retention time of 33.0 min, M+ at *m/z* 595.2 and fragment ions at *m/z* 449.1 and 287.0, was identified as cyanidin 3-rutinoside (45.3%). Peak 3, with a retention time of 36.4 min, M+ at *m/z* 433.1 and a fragment ion at *m/z* 271.0, was identified as pelargonidin 3-glucoside (2.1%). Peak 4, with a retention time of 38.0 min, M+ at *m/z* 579.1 and fragment ions at *m/z* 433.1 and 271.0, was identified as pelargonidin 3-rutinoside (1.2%). The results of the UV-Vis quantification of the total ANC content showed that the phenolic-rich extract contained 28 mg/g of total ANCs (calculated as cyanidin-3-O-glucoside equivalents). The total phenolic content of ANC extracts, expressed as mmol of Fe(II) equivalents and gallic acid equivalents, was 67.28 GAEmM/Gfw and 22.67 FeFmM/gFW, respectively (data not shown).

Hypoglycemic effects of ANCs and histology of pancreatic islets in ZDF rats. Table II shows the changes in body weight observed in the six groups of rats. The ZDF rats had significantly higher body weights than their lean littermates from 8 weeks of age, and the body weight progressively increased with age ($P<0.05$). ANC treatment did not affect body weight in either genotype. Moreover, following 4 weeks of treatment, ZDF rats treated with 250 mg/kg ANCs tended to gain more weight than those treated with CMC alone or with 125 mg/kg ANCs, although this was not statistically significant ($P=0.3$ versus CMC; $P=0.11$ versus 125 mg/kg ANCs).

Blood glucose levels were measured in all of the rats for 5 weeks prior to the commencement of the study and throughout the experimental period (Fig. 2A). At 7 weeks of age, the ZDF rats treated with the vehicle showed mild hyperglycemia (~159 mg/dl) that rapidly progressed, reaching levels of ~396 mg/dl after 3 weeks. The administration of ANCs did not affect the glucose levels in the lean rats. Glucose levels increased significantly from 105.5±8.7 mg/dl at 0 weeks to 396.25±21 mg/dl ($P<0.0001$) at 5 weeks in the ZDF rats treated with CMC; however, the glucose levels were significantly lower in the rats treated with 125 and 250 mg/kg ANCs (228.25±45 and 131.75±10 mg/dl, respectively; $P<0.001$ for each; Fig. 2B). Treatment with 250 mg/kg ANCs reduced glucose levels in the ZDF rats to values similar to those in their lean littermates (Fig. 2).

At the start of treatment, when the rats were 5 weeks of age, plasma insulin levels were significantly higher in the ZDF rats than in the lean rats (11±0.2 versus 4.2±0.0 pg/ml; $P<0.001$; Fig. 3). Between 0 and 5 weeks, the insulin levels decreased from 10.88±0.0 to 7.9±0.4 ng/ml ($P<0.05$) in the CMC-treated ZDF rats, and from 11.51±0.0 to 8.72±1.4 ng/ml ($P<0.05$) in the ZDF rats treated with 125 mg/kg ANCs. Notably, plasma insulin levels did not decrease in the ZDF rats treated

Table I. Identification of anthocyanins (ANCs) in mulberry fruit.

Compound number[a]	Retention time (min)	MS, M+ (*m/z*)	MS/MS (*m/z*)	Assignment[b]
1	31.3	449.1	287.0	Cyanidin 3-O-glucoside
2	33.0	595.2	449.1/287.0	Cyanidin 3-rutinoside
3	36.4	433.1	271.0	Pelargonidin 3-glucoside
4	38.0	579.1	433.1/271.0	Pelargonidin 3-rutinoside

[a]Diode array detection at 350 nm; [b]Based on the fragmentation pattern and its aglycone. The assay was performed in triplicate. MS, mass spectrometry.

Table II. Changes in body weight in each experimental group.

	Body weight (g)			
Group	0 weeks	2 weeks	4 weeks	5 weeks
Lean rats				
+1% CMC	124±6	152±2	226±6	277±10
+125 ANCs	121±13	153±6	226±4	288±15
+250 ANCs	118±5	149±7	211±11	270±13
ZDF rats				
+1% CMC	143±2	182±4	256±30	324±24
+125 ANCs	139±3	187±6	257±9	317±34
+250 ANCs	140±6	188±6	273±15	331±7

ZDF, Zucker diabetic fatty; +1% CMC, treated with 1% carboxymethylcellulose; +125 ANCs, treated with 125 mg anthocyanins/kg body weight; +250 ANCs, treated with 250 mg anthocyanins/kg body weight.

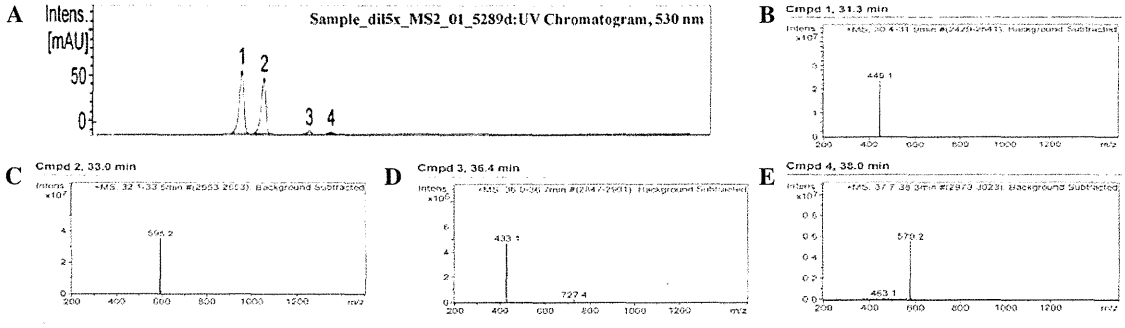

Figure 1. High-performance liquid chromatography (HPLC)-electrospray ionization (ESI)-mass spectometry (MS) analysis of mulberry anthocyanins (ANCs). (A) Chromatogram for the ANC extract of mulberry fruit at 520 nm. Four peaks were detected with retention times ranging from 31 to 38 min. Chromatograms for (B) cyanidin 3-O-glucoside, (C) cyanidin 3-rutinoside, (D) pelargonidin 3-glucoside and (E) pelargonidin 3-rutinoside. The parameters used for peak identification are listed in Table I. Intens, intensity; Cmpd, compound.

with 250 mg/kg ANCs (0 weeks: 10.8±0.6 ng/ml; 5 weeks: 10.93±0.4 ng/ml).

A histological evaluation of the pancreatic islets of 10-week-old ZDF and lean rats was also conducted. H&E staining revealed no significant pathological abnormalities in the islets from the lean rats, which were round or oval with well-defined boundaries (Fig. 4A-C). However, histological examination of the pancreatic islets from the CMC-treated ZDF rats revealed substantial changes in islet morphology. In particular, the islets were hypertrophic and compressed adjacent exocrine tissue, and there was marked vascular congestion or hemorrhagic degeneration (Fig. 4D, upper panel). Furthermore, the islets were disorganized, with finger-like projections into the surrounding exocrine tissue. The degenerated islets also showed β-cell vacuolation and degeneration (Fig. 4D, lower panel). By contrast, the histological assessment of pancreatic sections from the ZDF rats treated with 125 mg/kg ANCs showed a normal distribution

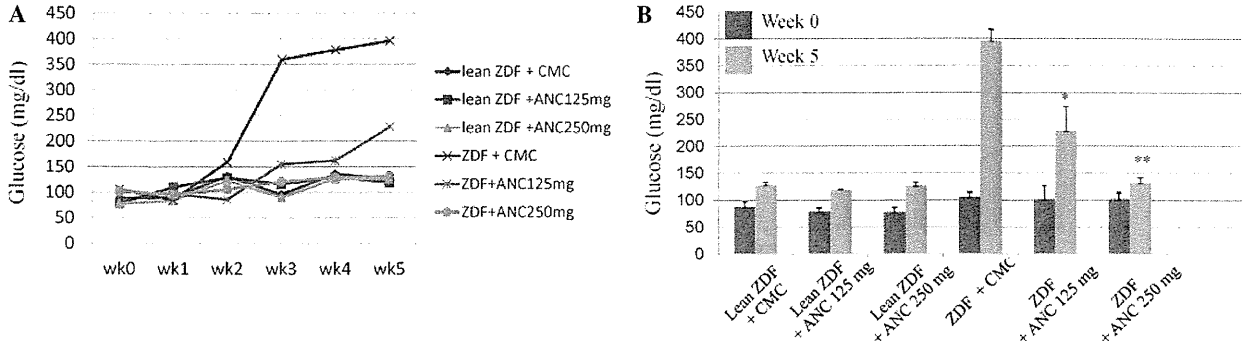

Figure 2. Blood glucose levels of Zucker diabetic fatty (ZDF) and lean ZDF rats treated with 125 or 250 mg/kg anthocyanin (ANC) or 1% carboxymethylcellulose (CMC; vehicle control). (A) Blood glucose levels measured every week during the experimental period. ANCs lowered the glucose levels in the ZDF rats within 3 weeks of treatment in comparison with the levels in the CMC-treated rats. (B) Change in glucose levels from week 0 to week 5. The results are shown as the mean ± standard deviation (n=3-5 rats/group). *P<0.001 and **P<0.0001 vs. CMC-treated ZDF rats.

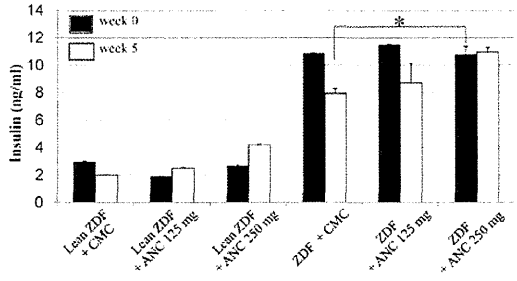

Figure 3. Plasma insulin levels in Zucker diabetic fatty (ZDF) and lean ZDF rats treated with 125 or 250 mg/kg anthocyanin (ANC) or 1% carboxymethylcellulose (CMC) for 5 weeks. Plasma insulin levels at week 0 were significantly higher in the ZDF rats than in their lean littermates (P<0.001). The insulin secretion in the 250 mg/kg ANC-treated ZDF rats at week 5 was 27% higher than that in the CMC-treated ZDF rats. The results are shown as the mean ± standard deviation (n=3-5 rats/group). *P<0.001.

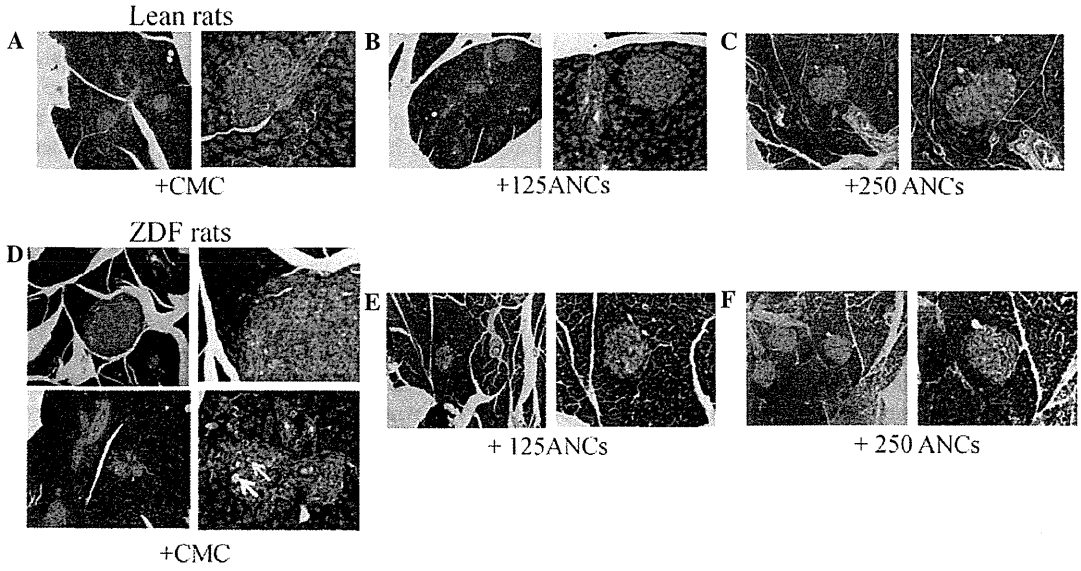

Figure 4. Representative hematoxylin/eosin (H&E)-stained pancreas tissue sections from 11-week-old obese Zucker diabetic fatty (ZDF) and lean rats treated with 125 or 250 mg/ml anthocyanin (ANC) or 1% carboxymethylcellulose (CMC). (A-C) There were no pathological abnormalities in the islets of lean rats. The islets consisted of small, rounded aggregates of mildly eosinophilic cells and were regularly shaped with well-defined boundaries. (D) There were marked morphological changes in the islets of obese ZDF rats, as the islets were hypertrophied and compressed adjacent exocrine tissue, resulting in vascular congestion and hemorrhage. The islets were also disorganized, with extensions into the surrounding exocrine tissue. The degenerated islets showed β-cell vacuolation and degeneration (arrows). (E) Islets of ZDF rats treated with 125 mg/kg ANC showed a normal distribution within the exocrine tissue and mild β-cell vacuolation. (F) There were substantially fewer degenerated islets in ZDF rats treated with 250 mg/kg ANC. The islets in these rats were regularly shaped with well-defined boundaries. H&E staining; original magnification, x100 (left image) and x200 (right image).

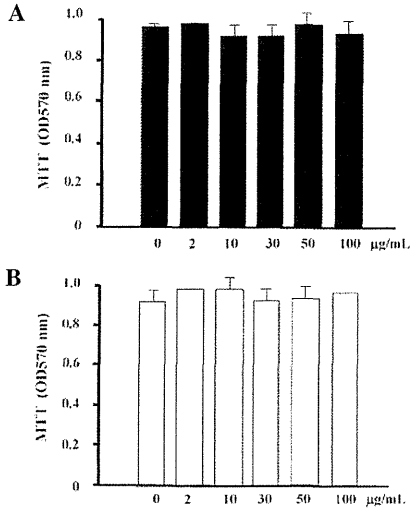

Figure 5. Cytotoxic effect of anthocyanins (ANCs) on (A) murine macrophages and (B) rat kidney cells. Cells were exposed to the indicated concentration of ANC for 48 h and cell viability was quantified using an MTT assay. The results are shown as the mean ± standard deviation for two separate experiments, with each condition performed in duplicate.

of islets within the exocrine tissue and some β-cell vacuolation (Fig. 4E). Notably, the evaluation of the pancreatic tissue samples collected from the ZDF rats treated with 250 mg/kg ANCs suggested that this dose had certain protective effects, since there were fewer abnormal morphological features and fewer degenerated islets. Additionally, the islets demonstrated a regular shape with well-defined boundaries (Fig. 4F).

In the cell culture studies, it was observed that the ANCs did not exert any cytotoxic effects on the murine macrophages or rat kidney cells (Fig. 5).

Discussion

The results from this study suggest that ANCs extracted from mulberry fruit exhibit significant anti-diabetic properties by improving blood glucose levels in ZDF rats as an animal model of type 2 diabetes. To the best of our knowledge, this has shown for the first time that ANCs are able to attenuate islet degeneration in ZDF rats. The results demonstrating that ANCs reduced blood glucose levels were consistent with those of a prior study showing that ANCs extracted from black soybean seed coats exhibited antidiabetic and antioxidative effects in streptozotocin-induced diabetic rats (22). Furthermore, the administration of ANCs extracted from *Calendula officinalis* fruits has been demonstrated to significantly increase insulin release from pancreatic β-cells *in vitro* (8).

In the present study, the chromatogram of the purified product following acid hydrolysis of the ethanol extract revealed that cyanidin 3-O-glucoside (51.4%) and cyanidin-3-rutinoside (45.3%) were the major ANCs present in Thai *Morus alba L.* The minor ANCs, which comprised 3.3% of the total ANCs, were pelargonidin 3-O-glucoside and pelargonidin 3-O-rutinoside. These results were consistent with those revealed in the study by Qin *et al* (23), although the ANC content differed, most likely due to differences between mulberry species and cultivars, as well as differences in extraction, separation, purification and analysis between the two studies.

Lean ZDF rats have been demonstrated to be less sensitive to exogenous glucose-induced hyperglycemia (23). The ZDF rats in the present study exhibited marked hyperglycemia at 7 weeks of age and their blood glucose levels continued to increase with age. These results were consistent with those of a previous study in which diabetes occurred spontaneously in male rats aged ~6 weeks, and was associated with hyperphagia, polyuria and polydipsia (24). It was also revealed that the β-cell mass decreased by 51% from 9 to 12 weeks of age (24). In rats aged 6-12 weeks, the β-cell mass is not able compensate for insulin resistance, resulting in compensatory β-cell proliferation (25).

In a previous study, treatment with the ANC cyanidin 3-O-glucoside reduced the body weight and fat accumulation in visceral adipose and liver tissues of KK-Ay mice by improving triglyceride metabolism and regulating lipoprotein lipase activity (26). In another study, aqueous mulberry extract exhibited anti-obesity effects by upregulating hepatic peroxisome proliferator-activated receptor α and carnitine palmitoyltransferase-1 expression, and reducing fatty acid synthase and 3-hydroxy-3-methylglutaryl-coenzyme A (HMG-CoA) reductase expression (14). However, in the present study, the ANC extract from mulberry fruit did not promote reductions in body weight. In fact, the dose of 250 mg/kg ANCs resulted in a certain level of weight gain in the ZDF rats from the age of 9 weeks ($P>0.05$), without changes in food intake. The differences in results may be due to differences in the polyphenols contained in the extracts or their free radical scavenging properties and mechanisms of action.

To the best of our knowledge, this study has demonstrated for the first time that mulberry fruit extract contains abundant cyanidin 3-O-glucoside (~28 mg/g of crude ANC extract), with the highest ANC dose (250 mg/kg body weight) containing ~7 mg cyanidin 3-O-glucoside. Blood glucose levels were 66% lower and insulin levels were 27% higher in the ZDF rats treated with 250 mg/kg ANCs than in those treated with CMC between 5 and 10 weeks of age. In addition, the consumption of ANCs did not affect glycemia in lean rats. The maximum dose of ANCs used in this study was derived from the cyanidin 3-O-glucoside concentration (10 mg/kg) used in a prior study (11). To date, there are limited data on the mechanisms of ANCs with regard to insulin-mediated glucose uptake. Certain studies have shown that cyanidin 3-O-glucoside from black beans significantly upregulated glucose transport 4 (GLUT4) expression, induced adipocyte differentiation and glucose uptake *in vitro* (27), and prevented insulin resistance and pancreatic apoptosis in streptozotocin-induced diabetic rats (28).

In the present study, the islets of the lean rats showed normal histological features. By contrast, there were marked morphological changes, including islet hypertrophy and cellular degeneration, in the CMC-treated ZDF rats. These pathological observations were consistent with those of earlier studies showing pancreatic islet hypertrophy in ZDF rats (29). By the time diabetes is diagnosed, β-cells attempt to secrete sufficient insulin to overcome the insulin resistance in a process that involves islet hyperplasia. Degenerating islet

cells show cytoplasmic vacuolation, possibly resulting from autodigestion following cell death (25). In the present study, the histological assessment of the pancreatic islets from the ZDF rats demonstrated that 250 mg/kg ANCs attenuated the degenerative changes in the majority of the rats. Furthermore, the ANC extract prevented marked reductions in the plasma insulin levels in these rats. These effects may be coupled with enhanced hepatic/peripheral tissue glucose uptake. It was not possible to clarify the mechanism from the current results. Further studies are required to identify the mechanisms of action of ANCs using isolated islets or β-cells to examine whether ANCs have direct effects on insulin secretion.

In conclusion, our results suggest that the ANC extract of mulberry fruit is an effective anti-diabetic agent with marked glucose-lowering effects that prevents the progressive decline in insulin secretion. Although ANCs may protect against β-cell damage, further studies are required to examine the pharmacokinetics and the molecular basis for the pharmacological activity of ANCs on insulin resistance and glucose handling in the management of diabetes mellitus. Long-term studies are required to confirm the present results and to establish the durability of the improvements in glucose levels.

Acknowledgements

This study was supported in part by a grant from the SENSHIN Medical Research Foundation. The authors would like to thank Ms. Pornpen Dararat, Dr Yuko Nawa, Dr Fumiyo Masuda, Ms. Tomoka Nagasato, Ms. Mika Yamamoto, Ms. Nobue Uto and all the staff at the Department of Laboratory and Vascular Medicine, Kagoshima University (Kagoshima, Japan) and the Department of Pharmacology, Faculty of Dentistry, Mahidol University (Bangkok, Thailand), for their assistance with the experiments.

References

1. Jun H, Bae HY, Lee BR, *et al*: Pathogenesis of non-insulin-dependent (type II) diabetes mellitus (NIDDM) - genetic predisposition and metabolic abnormalities. Adv Drug Deliv Rev 35: 157-177, 1999.
2. Rosak C: The pathophysiologic basis of efficacy and clinical experience with the new oral antidiabetic agents. J Diabetes Complications 16: 123-132, 2002.
3. Jennings AM, Wilson RM and Ward JD: Symptomatic hypoglycemia in NIDDM patients treated with oral hypoglycemic agents. Diabetes Care 12: 203-208, 1989.
4. Xia X, Ling W, Ma J, *et al*: An anthocyanin-rich extract from black rice enhances atherosclerotic plaque stabilization in apolipoprotein E-deficient mice. J Nutr 136: 2220-2225, 2006.
5. Wallace TC: Anthocyanins in cardiovascular disease. Adv Nutr 2: 1-7, 2011.
6. Wang LS and Stoner GD: Anthocyanins and their role in cancer prevention. Cancer Lett 269: 281-290, 2008.
7. Grace MH, Ribnicky DM, Kuhn P, *et al*: Hypoglycemic activity of a novel anthocyanin-rich formulation from lowbush blueberry, *Vaccinium angustifolium* Aiton. Phytomedicine 16: 406-415, 2009.
8. Jayaprakasam B, Vareed SK, Olson LK and Nair MG: Insulin secretion by bioactive anthocyanins and anthocyanidins present in fruits. J Agric Food Chem 53: 28-31, 2005.
9. Duthie G and Crozier A: Plant-derived phenolic antioxidants. Curr Opin Clin Nutr Metab Care 3: 447-451, 2000.
10. Kaewkaen P, Tong-Un T, Wattanathorn J, *et al*: Mulberry fruit extract protects against memory impairment and hippocampal damage in animal model of vascular dementia. Evid Based Complement Alternat Med 2012: 263520, 2012.
11. Andallu B, Kumar AV and Varadacharyulu NC: Oxidative stress in streptozocin-diabetic rats: Amelioration by mulberry (*Morus Indica* L.) leaves. Chin J Integr Med Dec. 22, 2012 (Epub ahead of print).
12. Musabayane CT, Bwititi PT and Ojewole JA: Effects of oral administration of some herbal extracts on food consumption and blood glucose levels in normal and streptozotocin-treated diabetic rats. Methods Find Exp Clin Pharmacol 28: 223-228, 2006.
13. Du Q, Zheng J and Xu Y: Composition of anthocyanins in mulberry and their antioxidant activity. J Food Compost Anal 21: 390-395, 2008.
14. Peng CH, Liu LK, Chuang CM, Chyau CC, Huang CN and Wang CJ: Mulberry water extracts possess an anti-obesity effect and ability to inhibit hepatic lipogenesis and promote lipolysis. J Agric Food Chem 59: 2663-2671, 2011.
15. Chen PN, Chu SC, Chiou HL, Kuo WH, Chiang CL and Hsieh YS: Mulberry anthocyanins, cyanidin 3-rutinoside and cyanidin 3-glucoside, exhibited an inhibitory effect on the migration and invasion of a human lung cancer cell line. Cancer Lett 235: 248-259, 2006.
16. Ha US, Bae WJ, Kim SJ, *et al:* Protective effect of cyanidin-3-O-β-D-glucopyranoside fraction from mulberry fruit pigment against oxidative damage in streptozotocin-induced diabetic rat bladder. Neurourol Urodyn Nov. 25, 2012 (Epub ahead of print).
17. Clark JB, Palmer CJ and Shaw WN: The diabetic Zucker fatty rat. Proc Soc Exp Biol Med 173: 68-75, 1983.
18. Mega C, de Lemos ET, Vala H, *et al*: Diabetic nephropathy amelioration by a low-dose sitagliptin in an animal model of type 2 diabetes (Zucker diabetic fatty rat). Exp Diabetes Res 2011: 162092, 2011.
19. Yu X, Zhao M, Hu J, Zeng S and Bai X: Correspondence analysis of antioxidant activity and UV-Vis absorbance of Maillard reaction products as related to reactants. LWT - Food Science and Technology 46: 1-9, 2012.
20. Zhang M, Chen H, Li J, Pei Y and Liang Y: Antioxidant properties of tartary buckwheat extracts as affected by different thermal processing methods. LWT - Food Science and Technology 43: 181-185, 2010.
21. Sutharut J and Sudarat J: Total anthocyanin content and antioxidant activity of germinated colored rice. International Food Research Journal 19: 215-221, 2012.
22. Nizamutdinova IT, Jin YC, Chung JI, *et al*: The anti-diabetic effect of anthocyanins in streptozotocin-induced diabetic rats through glucose transporter 4 regulation and prevention of insulin resistance and pancreatic apoptosis. Mol Nutr Food Res 53: 1419-1429, 2009.
23. Qin C, Li Y, Niu W, Ding Y, Zhang R and Shang X: Analysis and characterisation of anthocyanins in mulberry fruit. Czech J Food Sci 28: 117-126, 2010.
24. Jones HB, Nugent D and Jenkins R: Variation in characteristics of islets of Langerhans in insulin-resistant, diabetic and non-diabetic-rat strains. Int J Exp Pathol 91: 288-301, 2010.
25. Pick A, Clark J, Kubstrup C, Levisetti M, Pugh W, Bonner-Weir S and Polonsky KS: Role of apoptosis in failure of beta-cell mass compensation for insulin resistance and beta-cell defects in the male Zucker diabetic fatty rat. Diabetes 47: 358-364, 1998.
26. Wei X, Wang D, Yang Y, *et al*: Cyanidin-3-O-β-glucoside improves obesity and triglyceride metabolism in KK-Ay mice by regulating lipoprotein lipase activity. J Sci Food Agric 91: 1006-1013, 2011.
27. Inaguma T, Han J and Isoda H: Improvement of insulin resistance by Cyanidin 3-glucoside, anthocyanin from black beans through the up-regulation of GLUT4 gene expression. BMC Proc 5 (Suppl 8): P21, 2011.
28. Nizamutdinova IT, Jin YC, Chung JI, Shin SC, Lee SJ, Seo HG, Lee JH, Chang KC and Kim HJ: The anti-diabetic effect of anthocyanins in streptozotocin-induced diabetic rats through glucose transporter 4 regulation and prevention of insulin resistance and pancreatic apoptosis. Mol Nutr Food Res 53: 1419-1429, 2009.
29. Janssen SW, Hermus AR, Lange WP, *et al*: Progressive histopathological changes in pancreatic islets of Zucker Diabetic Fatty rats. Exp Clin Endocrinol Diabetes 109: 273-282, 2001.

Upregulation of non-β Cell-derived Vascular Endothelial Growth Factor A Increases Small Clusters of Insulin-producing Cells in the Pancreas

One Sentence Summary: The authors showed that upregulation of non-beta cell-derived VEGF-A increased the number of small clusters of insulin producing cells without forming islets in mice, which suggests new functions of non-beta cell-derived VEGF-A to insulin producing cell regeneration and insulin production.

Authors

K. Takenouchi[1], B. Shrestha[1], M. Yamakuchi[1], N. Yoshinaga[2], N. Arimura[2], H. Kawaguchi[3], T. Nagasato[4], R. Feil[5], K.-i. Kawahara[6], T. Sakamoto[2], I. Maruyama[4], T. Hashiguchi[1]

Affiliations

Affiliation addresses are listed at the end of the article

Key words
- diabetes
- islet
- smooth muscle cell
- streptozotocin

Abstract

Background: Pancreatic β cell-derived vascular endothelial growth factor A (VEGF-A) contributes to normal β cell function. We therefore hypothesized that non-β cell-derived VEGF-A may affect its properties in adult mice.

Methods: We generated transgenic mice expressing human VEGF-A (hVEGF-A) in a visceral smooth muscle cell (SMC)-dominant manner under the control of the transgelin (*Tagln/SM22α*) promoter *via* a tamoxifen-induced Cre/loxP recombination system (SM-CreER^{T2}/hVEGF mice).

SM-CreER^{T2}/hVEGF mice received tamoxifen orally followed by microscopic examination of their pancreas 4 weeks after the hVEGF-A induction. The number of clusters of insulin-producing cells (IPCs) in islets, pancreatic ducts, and individual IPCs were counted.

Results: The number of small IPC clusters (100–215 μm^2) in the pancreas increased significantly in SM-CreER^{T2}/hVEGF mice compared to SM-CreER^{T2}(Ki) mice (473 out of 1 992 counts vs. 199 out of 976 counts, $p<0.05$), although total IPC area and the number of pancreatic duct IPCs, in proportion to exocrine area, were similar between the 2 groups. Although most small IPC clusters observed in SM-CreER^{T2}/hVEGF mice were not accompanied by α and/or δ cells, some were attached to a single or a few α cells. An STZ-induced diabetic state in SM-CreER^{T2}/hVEGF mice was slightly ameliorated, with only one point of significance 12 weeks after STZ administration, compared to SM-CreER^{T2}(Ki) mice.

Conclusion: Upregulation of non-β cell-derived VEGF-A may alter the composition of pancreatic IPCs by increasing the number of small IPC clusters. These findings provide new information on the role of non-β cell-derived VEGF-A to IPC regeneration and insulin production.

received 06.02.2014
first decision 06.02.2014
accepted 26.02.2014

Bibliography
DOI http://dx.doi.org/10.1055/s-0034-1371811
Exp Clin Endocrinol Diabetes 2014; 122: 1–8

ISSN 0947-7349

Correspondence
T. Hashiguchi, MD, PhD
Department of Laboratory and Vascular Medicine
Kagoshima University Graduate School of Medical and Dental Sciences
8-35-1, Sakuragaoka
Kagoshima 890-8520
Japan
Tel.: +81/99/275/5437
Fax: +81/99/275/2629
terutoha@m3.kufm.kagoshima-u.ac.jp

Introduction

Several studies have demonstrated a relationship between islet vascularization and function. Normal islets are highly vascularized and contain fenestrated endothelium. During embryonic development, the pancreatic endothelium signals pancreatic islets to develop. Subsequently, islet cells signal back to the vascular endothelium to form a branching network of capillaries in the growing islets [1]. Because vascular endothelial growth factor A (VEGF-A) is a key molecule for angiogenesis, the role of VEGF-A in islet vascularization has been studied intensively. Lammert et al. reported that VEGF-A was not required for the development of islet capillaries, but that it induced a capillary network essential for the fine-tuning of blood glucose regulation [2]. In addition, Brissova et al. showed that VEGF-A was a major regulator of islet vascularization and revascularization of transplanted islets [3]. Islet VEGF-A expression is thus thought to be essential for maintaining normal islet vascularization and function. Although most of these experiments have been conducted using a β-cell-specific VEGF-A-deficient/over expression model, the biological effect of upregulated non-β cell-derived VEGF-A on its properties in vivo has not been investigated. Therefore, we generated transgenic mice expressing hVEGF-A in a visceral smooth muscle cell (SMC)-dominant manner, under the control of the transgelin (*Tagln/SM22α*) promoter and a tamoxifen-induced Cre/loxP recombination system (SM-CreER^{T2}/hVEGF mice) [4], to examine its role in the pancreas. Using these mice, we demonstrate that upregulation of non-β cell-derived VEGF-A increased the number of small clusters of IPCs without forming islets,

which suggests new functions of non-β cell-derived VEGF-A to IPC regeneration and insulin production.

Materials and Methods

Animals

Mice were kept in environmentally controlled pathogen-free conditions (lights on from 7:00 to 19:00; 23 °C; 55% humidity) with ad libitum access to water and a standard rodent diet. Animal experiments were performed according to the guidelines of the Natural Science Center for Research and Education, Kagoshima University. SM-CreER^{T2} (ki) mice carrying a *Tagln* knock-in allele, which expresses CreER^{T2} recombinase in response to tamoxifen administration, instead of the endogenous *Tagln* gene, were provided by Dr. Robert Feil [5].

Establishment of SM-CreER^{T2}/hVEGF mice

The plasmid construct containing human *VEGFA* flanked by a second *loxP* site (p-hVEGF-A^{fl}) is shown in ○ **Fig. 1**. To construct p-hVEGF-A^{fl}, the *lacZ* gene in pCETZ-17 was replaced by a 576-bp cDNA encoding human *VEGFA* [6]. The resulting DNA construct (p-hVEGF-A^{fl}) contained a CMV enhancer/chicken β-actin promoter (CAG), and an enhanced green fluorescent protein (EGFP)/chloramphenicol acetyltransferase (CAT) flanked by 2 *loxP* sites. The 5.4-kb *Spe I* fragment containing the hVEGF-A^{fl} transgene was removed from the p-hVEGF-A^{fl} vector and microinjected into fertilized egg pronuclei from C57BL/6N mice [6]. Transgenic founder (F0) mice (hVEGF-A^{fl} mice) were identified by EGFP-fluorescent blood cells using flow cytometry [7].

The presence of the hVEGF-A^{fl} transgene was confirmed by PCR with primers *Chi5'* (5'-GGC GGG GTT CGG CTT CTG GCG TGT GAC CGG-3') and *Veg3'* (5'-TCA CCG CCT CGG CTT GTC ACA TCT GCA AGT-3'), which recognize the chicken β-actin promoter and *VEGFA*, respectively. All F0 transgenic mice were crossed with wild-type C57BL/6N mice (aged 12–20 weeks). SM-CreER^{T2} (ki) mice were mated with heterozygous hVEGF-A^{fl} mice to generate double transgenic offspring expressing Cre, which would then respond to tamoxifen administration in an SMC-specific manner (SM-CreER^{T2}/hVEGF mice).

Preparation and administration of tamoxifen

A 10-mg/mL tamoxifen stock solution for intraperitoneal injection was prepared and stored as described previously [4]. Tamoxifen-containing chow (200 mg/kg food) was prepared by mixing 100 g of powdered mouse food and 20 mg of ground tamoxifen tablets (AstraZeneca PLC, London, UK) before use. Mice were injected with 100 µL of tamoxifen stock solution (1 mg tamoxifen) intraperitoneally for 5 days or fed tamoxifen-supplemented diet for 5 days.

Blood analysis

Blood samples were obtained from the saphenous vein as described previously [8]. Mice were fasted for 8 h before measuring fasting blood glucose levels using an enzyme-electrode method (Glutest; Sanwa Kagaku Kenkyusho, Nagoya, Japan).

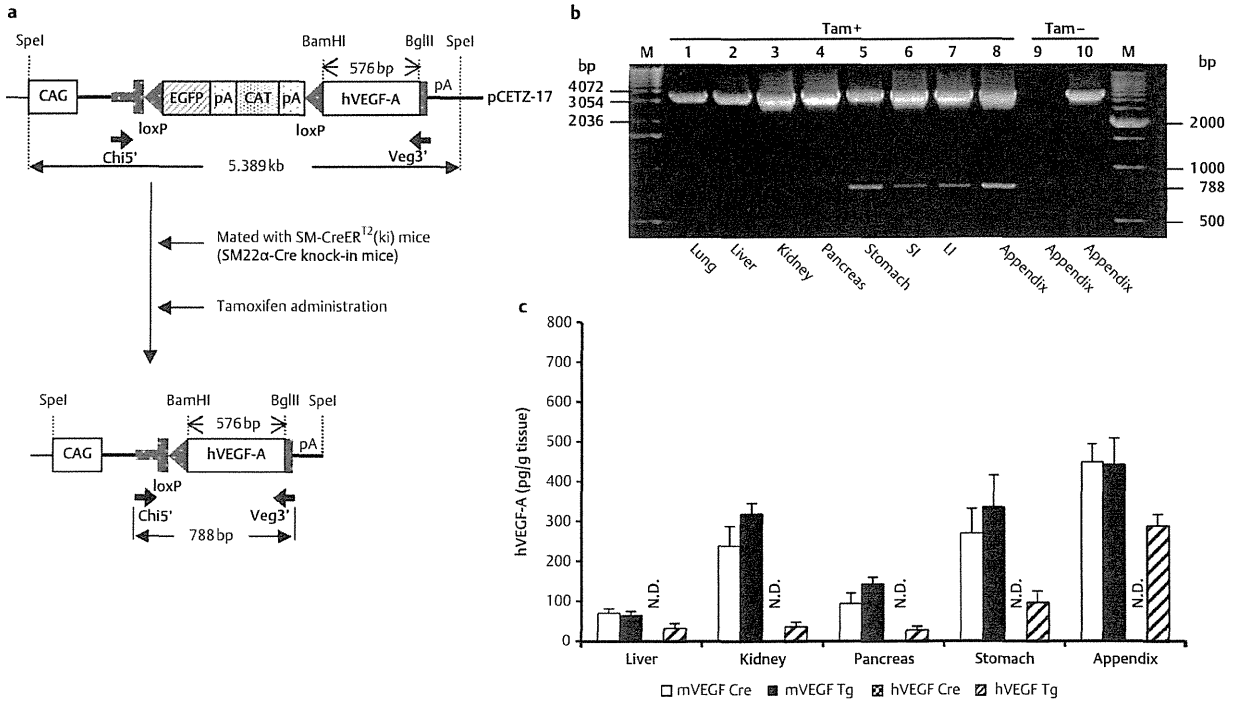

Fig. 1 DNA constructs and Cre-mediated recombination. **a** Schema of the target plasmid (p-hVEGF-A^{fl}) and its recombinant form. The *loxP* sites are shown as triangles. The small arrows (*Chi5'* and *Veg3'*) indicate the position and direction of the PCR primers. Tamoxifen was administrated orally except for **b** (where administration was intraperitoneally). **b** Identification of the Cre-mediated DNA recombination product by PCR amplification of DNA isolated from SM-CreER^{T2}/hVEGF (lanes 1–8), SM-CreER^{T2}(ki) (lane 9), and hVEGF^{fl} (lane 10) mice. The 788-bp fragment represents the recombinant DNA. M: size marker. Tam: tamoxifen. SI: small intestine. LI: large intestine. **c** Mouse and human VEGF-A protein expression in liver, kidney, pancreas, stomach and appendix vermiformis homogenate from SM-CreER^{T2}/hVEGF (Tg) (n=6) and SM-CreER^{T2}(ki) (Cre) (n=6) mice. N.D. = not detected.

VEGF-A expression analysis

To measure VEGF-A expression levels, liver, kidney, pancreas, stomach, and appendix (n=6) were lysed in RIPA lysis buffer (Santa Cruz Biotechnology, Santa Cruz, CA, USA) supplemented with protease inhibitors (Halt Protease Inhibitor Cocktail; Pierce Biotechnology, Rockford, IL, USA). Tissues were then sonicated on ice, and centrifuged at 10000×g for 10 min at 4 °C. Mouse and human VEGF-A concentrations in the supernatant was measured using a mouse or human VEGF ELISA kit (R&D Systems, Minneapolis, MN, USA), respectively.

Immunohistochemistry

Tissue samples were fixed in 10% phosphate-buffered formalin for 24 h at room temperature followed by paraffin embedding and examined by immunohistochemistry. Consecutive sections were incubated with rabbit anti-insulin (Cell Signaling Technology, Beverly, MA, USA; 1:200 dilution) followed by horseradish peroxidase-conjugated secondary antibody (Nichirei Bioscience, Tokyo, Japan). Staining was visualized with 3, 3′-diaminobenzidine (DAB) (DAKO, Carpinteria, CA, USA). Immunofluorescence was performed with chicken anti-insulin (Abcam, Cambridge, MA, USA; dilution 1:50), rabbit anti-glucagon (Cell Signaling Technology; 1:50), rabbit anti-somatostatin (ImmunoStar, Hudson, WI, USA; 1:400), or mouse anti-proliferating cell nuclear antigen (PCNA) (Cell Signaling Technology; 1:100) and subsequently incubated with fluorescently labeled secondary antibodies (Alexa Fluor 594, 488; Invitrogen, Carlsbad, CA, USA). The sections were examined under an ApoTome microscope (Carl Zeiss Inc., Oberkochen, Germany), and photographed with a charge-coupled device digital camera. Microscopic views were captured as digitized pictures using Axiovision software (Carl Zeiss Inc.). The area containing IPCs was analyzed using Image J 1.40 software (National Institute of Health, Bethesda, MD, USA). IPC clusters from 3–5 sections, obtained every 300 µm per pancreatic sample, were evaluated. The number of IPC clusters was counted and compared with that of control SM-CreER^{T2}(ki) mice.

Quantitative RT-PCR

Total RNA from tissues other than the pancreas was isolated with an RNAqueous Kit (Ambion, Austin, TX, USA). RNA extraction from pancreatic tissue was performed as described previously [9]. Briefly, pancreatic RNA samples were immediately frozen in liquid nitrogen and treated with RNAlater-ICE (Ambion). Total RNA was then isolated with an RNeasy Mini Kit (Qiagen, Valencia, CA, USA). For real-time quantitative RT-PCR (qRT-PCR), cDNA was reverse transcribed and amplified using TaqMan Gene Expression master mix on an ABI Prism 7300 (Applied Biosystems, Foster City, CA, USA). Expression levels of *Ins1* (Mm01259683_g1), *Ins2* (Mm00731595_g1), *Ngn3* (Mm00437606_s1), *Pdx1* (Mm00435565_m1), *Nkx6-1* (Mm00454962_m1), and *Mafa* (Mm00845206_s1) were normalized to *Gapdh* (Mm99999915_g1) expression.

Type I diabetes mice induced by streptozotocin

Mice were fasted for 8 h before inducing diabetes by STZ (Sigma, St. Louis, MO, USA) injection. STZ dissolved in saline on ice was administered intraperitoneally at a dose of 50 mg/kg body weight/day for 5 consecutive days. Mice not exhibiting diabetic symptoms received up to 3 additional 50 mg/kg of STZ doses, until fasting blood glucose levels of more than 300 mg/dL were reached.

Statistical analysis

Results are presented as mean±SEM. Statistical analyses were performed using unpaired Student's t-test. Values of $p<0.05$ were considered statistically significant.

Results

Generation of transgenic mice with SMC-specific hVEGF-A expression

We generated mice overexpressing hVEGF-A in SMC by crossing *loxP*-flanked EGFP mice (hVEGF-A^{fl}) with mice expressing Cre under the control of an SMC-specific promoter responding to tamoxifen (SM-CreER^{T2}(ki)) (○ **Fig. 1a**). Before recombination, the *loxP*-flanked EGFP/CAT hybrid sequence was expressed under control of the CAG promoter, while the *VEGFA* gene was silent [10]. All experiments were performed under tamoxifen administration and Cre-mediated recombination resulting in the deletion of the EGFP/CAT sequence and subsequent expression of *VEGFA*, resulting in SM-CreER^{T2}/hVEGF transgenic mice. The presence of a 788-bp PCR product from SM-CreER^{T2}/hVEGF mice confirmed successful recombination (○ **Fig. 1a, b**). The transgene recombination was predominantly observed in visceral smooth muscle cells (SMCs), such as the gastrointestinal tract (○ **Fig. 1b**).

Next, we examined hVEGF-A and mouse VEGF-A (mVEGF-A) protein levels in SM-CreER^{T2}/hVEGF mice. hVEGF-A was detected dominantly in the stomach and the appendix of SM-CreER^{T2}/hVEGF mice (97.9±72.5 or 290.5±74.3 pg/mg tissue, respectively; ○ **Fig. 1c**). Expression of hVEGF-A in SM-CreER^{T2}/hVEGF mice was moderate and hVEGF-A levels were less than mVEGF-A. hVEGF-A was not detected in the appendix of tamoxifen-treated SM-CreER^{T2}(ki) mice, suggesting there was no cross-reactivity between hVEGF and mVEGF by ELISA assay.

SM-CreER^{T2}/hVEGF mice appeared normal and had normal body weights and life spans. The proportions of SM-CreER^{T2}/hVEGF, SM-CreER^{T2}(ki), hVEGF-A^{fl}, and wild-type mice were in accordance with Mendelian ratios, at 26.2, 25.4, 20.7 and 27.7%, respectively.

Small clusters of insulin producing cells increased in SM-CreER^{T2}/hVEGF mice

Immunohistochemical examination was performed to determine the effect of enhanced SMC hVEGF-A expression on the pancreas. Morphologically distinct changes were not observed in pancreatic islets or exocrine tissues of tamoxifen-treated SM-CreER^{T2}/hVEGF mice, compared with tamoxifen-treated SM-CreER^{T2} (ki) mice. We did observe a number of small IPC clusters, in addition to pancreatic islets, in SM-CreER^{T2}/hVEGF mice (○ **Fig. 2a**). These IPCs were found as individual cells or as small clusters (○ **Fig. 2b**). The number of small IPC clusters (100–215 µm^2) in SM-CreER^{T2}/hVEGF mice increased significantly compared with SM-CreER^{T2} (ki) mice (473 out of 1992 clusters IPCs in SM-CreER^{T2}/hVEGF mice, n=5 vs. 199 out of 976 in SM-CreER^{T2} (ki) mice, n=3, $p<0.05$) (○ **Fig. 2c**). The proportion of IPC area, including small clusters of IPCs and islets, relative to exocrine area, was similar between SM-CreER^{T2}/hVEGF and SM-CreER^{T2} (ki) mice (○ **Fig. 2d**). In addition, the number of pancreatic duct IPCs relative to those that were exocrine based was similar (○ **Fig. 2e**). Double staining for glucagon or somatostatin and insulin was used to determine whether small IPC clusters consisted of only IPCs, or contained several types of endocrine

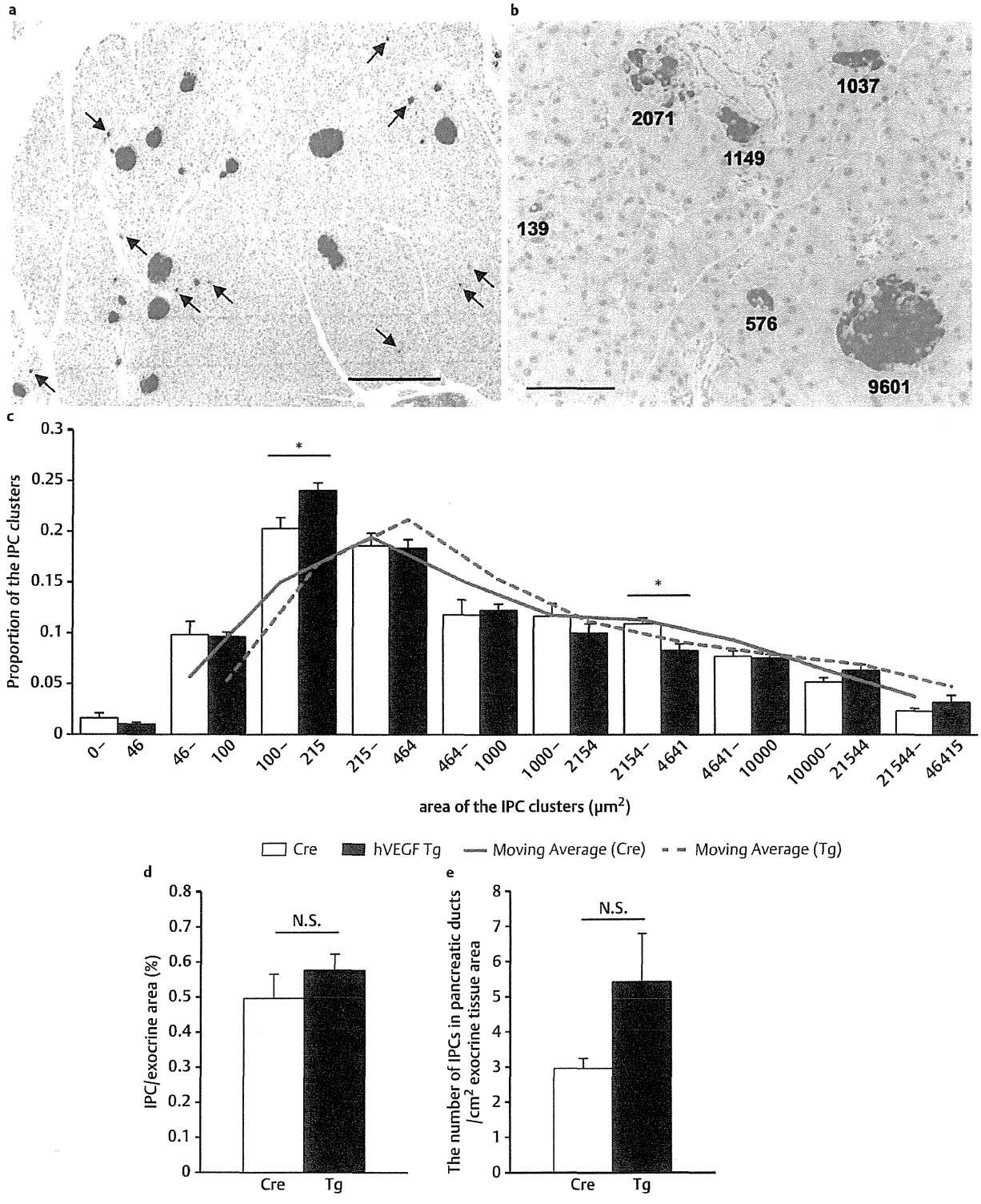

Fig. 2 Small IPC clusters increased in SM-CreER^{T2}/hVEGF mice, 4 weeks after hVEGF-A induction. **a** Immunohistochemistry of IPCs (brown) at 12 weeks of age; arrowheads: small IPC clusters. The scale bar indicates 500 μm. **b** The area of each IPC (μm²). The scale bar indicates 100 μm. **c** Proportion of IPC clusters according to size in 12-week-old mice. **d** IPC area over total exocrine area. **e** The number of IPCs in pancreatic ducts divided by total exocrine area (cm²). White bars: SM-CreER^{T2}(ki) (Cre) mice (976 IPC clusters in total, n = 3); black bars: SM-CreER^{T2}/hVEGF (Tg) mice (1992 IPC clusters in total, n = 5); Data represent mean ± SEM.*$p < 0.05$.

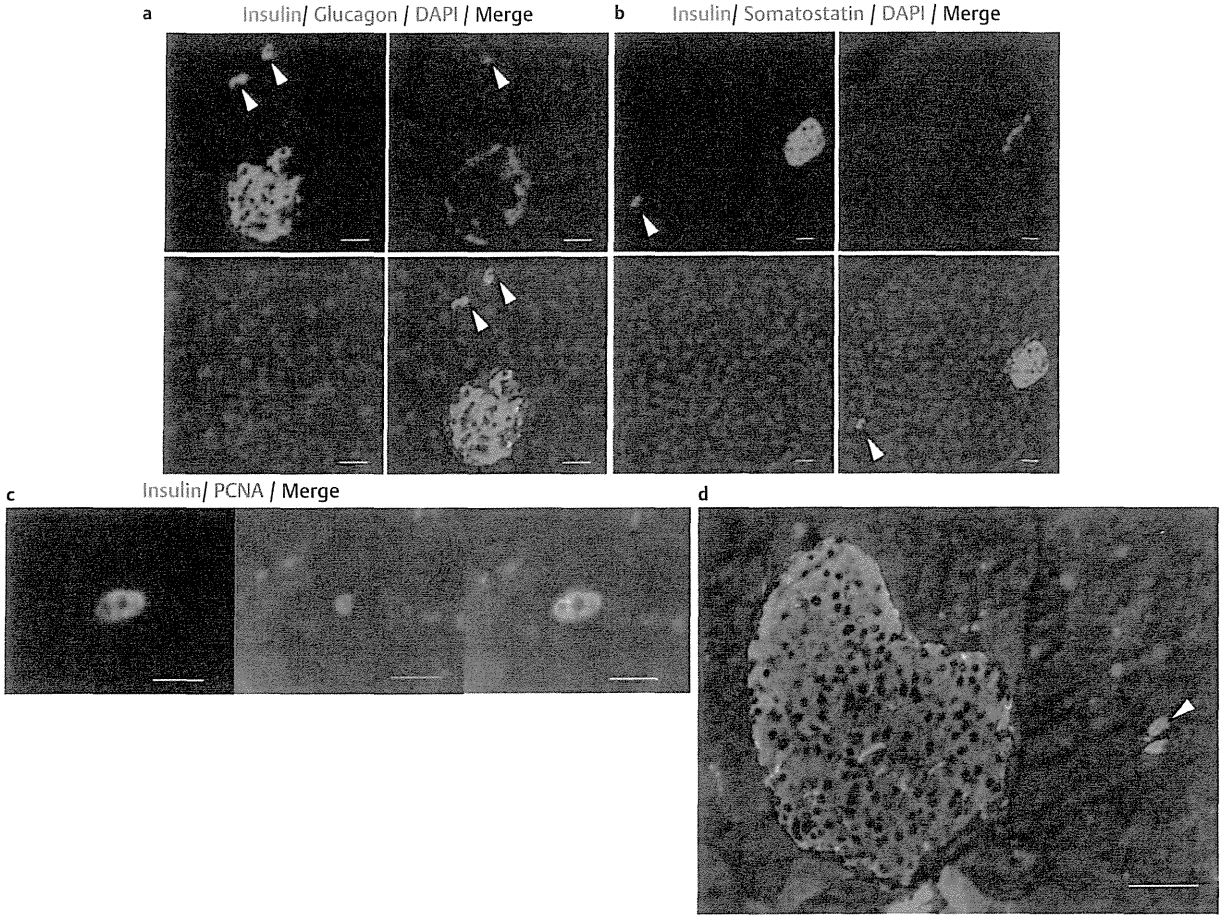

Fig. 3 Immunofluorescence for insulin (red; **a–d**), glucagon (green; **a**), somatostatin (green; **b**) and 4′,6-diamidino-2-phenylindole (DAPI) (blue; **a** and **b**) and PCNA (green; **c** and **d**) in SM-CreER^{T2}/hVEGF mice. Arrowheads: individual IPCs or small IPC clusters. The scale bars indicate 100 µm (**a** and **b**), 20 µm **c** and 50 µm **d**.

Table 1 Number of PCNA positive cells in SM-CreER^{T2} (ki) (Cre) mice and SM-CreER^{T2}/hVEGF (Tg) mice. The area of single IPCs or small IPC clusters was less than 215 µm^2. Pancreatic sections were obtained every 300 µm.

	number of mice	number of sections	PCNA positive cells	single/small clusters of IPCs
SM22α-Cre	3	15	0	380
hVEGF Tg	5	28	2	770

cells, as is usually observed in pancreatic islets. Immunofluorescence revealed that most small clusters contained only IPCs, with very few containing glucagon-producing cells (○ **Fig. 3a**). Somatostatin-producing cells attached to the small clusters were not observed (○ **Fig. 3b**). Insulin and PCNA staining was then used to investigate the proliferative capacity of small IPC clusters. 2 individual IPCs were PCNA positive in SM-CreER^{T2}/hVEGF mice out of 720 small IPC clusters (n=5, 28 sections). No PCNA positive cells were observed in SM-CreER^{T2} (ki) mice out of 380 small IPC clusters (n=3, 15 sections) (○ **Fig. 3c, d** and ○ **Table 1**).

Although regeneration of the β-cell mass in adult mice is reportedly due to replication of existing differentiated β-cells rather than progenitor cell differentiation, adult pancreatic stem or progenitor cells residing in pancreatic ducts, islets, or bone marrow [11–15]. To investigate the origin of IPC clusters, qRT-PCR analysis was performed for *Ins1*, *Ins2*, *Nkx6-1*, *Pdx1*, *Ngn3*, and *Mafa*, key molecules in β-cell differentiation [16–18]. Our qRT-PCR analysis showed that *Ngn3* and *Mafa* gene expression increased approximately 1.5 fold in SM-CreER^{T2}/hVEGF relative to SM-CreER^{T2} (ki) mice, although this was not statistically significant. The expression of other genes was comparable in SM-CreER^{T2}/hVEGF and SM-CreER^{T2} (ki) mice (○ **Fig. 4**).

Effects of non-β cell-derived VEGF-A in STZ-induced diabetic mice

We next investigated the long-term effects of non-β cell-derived VEGF-A over expression in STZ-induced diabetic mice [19] (○ **Fig. 5a**). We administered STZ (50 mg/kg body weight/day) to mice for 5 consecutive days until the blood glucose level exceeded 300 mg/dL. If blood glucose levels did not reach 300 mg/dL, an additional 50 mg/kg dose was administered (3 times at most). The total quantity of additional STZ between SM-CreER^{T2}/hVEGF and SM-CreER^{T2} (ki) mice was not statistically significant, with fasting blood glucose levels in SM-CreER^{T2}/hVEGF mice decreasing 3 weeks following hVEGF-A induction. However, a statistically significant improvement in fasting blood glucose, relative to diabetic SM-CreER^{T2} (ki) mice, was observed at only one point in the 12 weeks following STZ administration